

Article

Magmatic and post-magmatic evolution of the Newania carbonatite complex, Rajasthan, north-western India

Amritpaul Singh¹, Roger H. Mitchell² , Gurmeet Kaur¹ and D. Srinivasa Sarma³ 

¹Department of Geology, Panjab University, Chandigarh, India; ²Department of Geology, Lakehead University, Thunder Bay Ontario, Canada; and ³CSIR-National Geophysical Research Institute, Uppal Road, Hyderabad, India

Abstract

This work describes the mineralogy of dolomite carbonatite occurring at the Newania carbonatite complex, Rajasthan, north-western India. The mineralogy records the textural and compositional features of magmatic and post-magmatic stages of carbonatite evolution. Ferroan dolomite is the principal constituent and displays variable degrees of deformation, ranging from brittle-to-ductile deformation regimes. Apatite exhibits textural and compositional evolutionary trends from early-to-late stages of carbonatite evolution. Two varieties of amphibole are reported for the first time from this complex, ferri-winchite and cummingtonite; the former is magmatic and the latter is metamorphic in origin. The columbite-tantalite-series minerals are columbite-(Fe), and their paragenesis evolves from composite grains with pyrochlore to individual crystals. Pyrochlore is magmatic with U-Ta-Ti-rich compositions and shows evolution from calciopyrochlore to kenopyrochlore, followed by alteration during late-stages of carbonatite evolution. Monazite and baryte constitute the post-magmatic mineral assemblage; the former is hydrothermal and crystallised after precursor apatite, whereas the latter is associated exclusively with columbite-pyrochlore composites. On the basis of the mineralogy of the carbonatite, it is concluded that the parent magma was generated by low-degree partial melting of magnesite-phlogopite-bearing peridotite.

Keywords: carbonatite; mineralogy; Newania; Aravalli Craton; Rajasthan; India

(Received 17 May 2023; accepted 31 July 2023; Accepted Manuscript published online: 8 August 2023; Associate Editor: Leone Melluso)

Introduction

Carbonatites are igneous rocks which contain more than 50 modal percent igneous carbonate and less than 20 wt.% silica content (Le Maitre, 2002). Mitchell (2005, 2015) has redefined carbonatite as any igneous rock containing more than 30 vol.% primary carbonate, irrespective of its silica content. There are more than 500 carbonatite occurrences in world, ranging in age from Archean to Recent (Woolley and Kjarsgaard, 2008). These commonly occur in the continental crust and are tectonically associated with extensional and post-collisional settings (e.g. Mitchell and Smith, 2017; Boukrou et al., 2022). Calcite, dolomite, ferroan dolomite, magnesian siderite and siderite occur as the dominant carbonate minerals (Mitchell and Gittins, 2022) and can constitute up to 90 vol.% of the rock (Chudy, 2014). Accessory minerals include apatite, amphibole, phlogopite, magnetite, ilmenite, pyrite, baryte, fluorite and strontianite. Carbonatites are derived from mantle-derived magmas (e.g. Wallace and Green, 1988; Bell and Simonetti, 2010) and are known to host economic deposits of Nb (Mitchell, 2015) and rare earth elements (REE) (Chakhmouradian and Zaitsev, 2012).

The Newania carbonatite complex is one of the oldest carbonatite occurrences of more than 26 carbonatite localities in the Indian Peninsula. This is the only dolomite carbonatite-dominated occurrence with no associated calcite carbonatite and undersaturated

silicate rocks (Viladkar, 1980; Ray et al., 2013; Krishnamurthy, 2019; Tantkar, 2019). Subsequent to its first report as Aravalli limestone (Gupta, 1934), followed by identification as a carbonatite (Dar, 1964; Deans, unpublished report 1967), various petrologists have investigated the complex, mostly with respect to whole-rock geochemistry (Viladkar, 1980; Viladkar and Wimmenauer, 1986; Viladkar and Pawaskar, 1989; Pandit and Golani, 2001; Ray et al., 2010, 2013; Tantkar, 2019). Mineralogical aspects of the complex have been documented in Viladkar and Wimmenauer (1986), Buckley and Woolley (1990), Woolley and Buckley (1993), Viladkar and Ghose (2002), Doroshkevich et al. (2010a), Ray et al. (2013), Viladkar et al. (2017) and Sorokhtina et al. (2022). This study illustrates the petrographic and mineral compositional data for the constituent carbonate, silicate, phosphate and oxide minerals of the dolomite carbonatite to understand the magmatic and post-magmatic evolutionary history of the complex. The origin of the Newania carbonatites is briefly discussed as further data such as radiogenic isotopic studies are required.

Geological setting

Regional Geology

The Aravalli Craton is one of the five Precambrian cratons which constitute the Indian peninsula. This craton occupies the north-western region of India and is a part of the Aravalli orogen (Ramakrishnan and Vaidyanandhan, 2010). The Banded Gneissic Complex comprises the crystalline basement of the craton and has two subdivisions which lie south and north of Nathdwara,

Corresponding author: Amritpaul Singh; Email: apsbhatti05@gmail.com

Cite this article: Singh A., Mitchell R.H., Kaur G. and Sarma D.S. (2023) Magmatic and post-magmatic evolution of the Newania carbonatite complex, Rajasthan, north-western India. *Mineralogical Magazine* 87, 748–766. <https://doi.org/10.1180/mgm.2023.61>

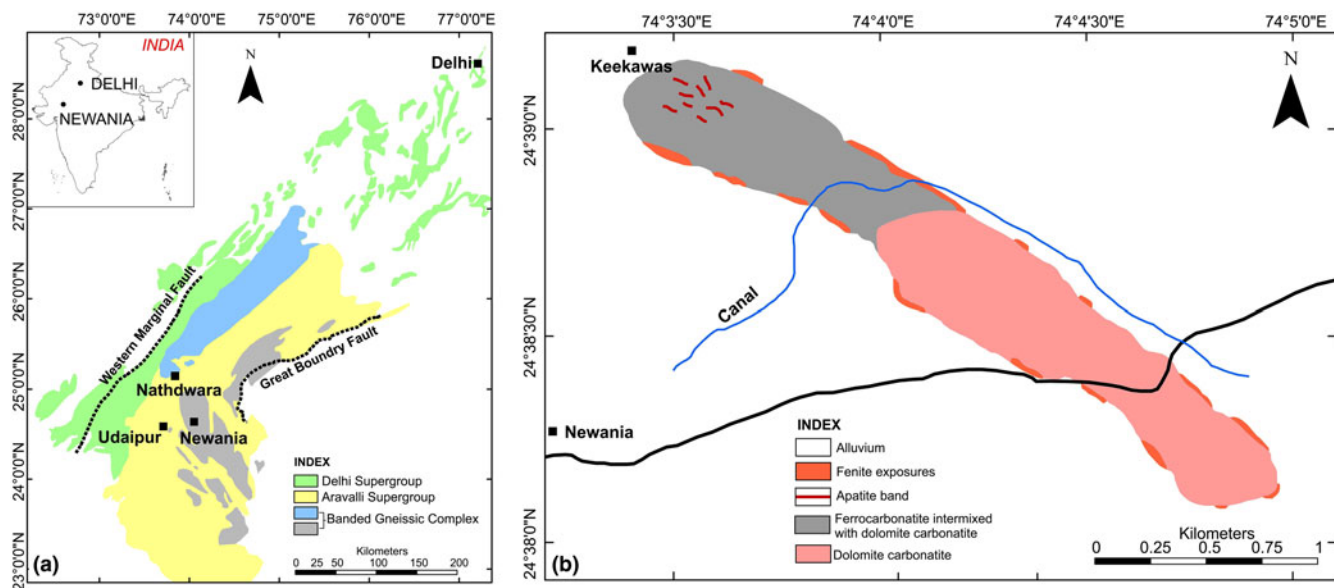


Figure 1. (a) Regional geological setting of the Aravalli Craton (after Heron, 1953; Roy and Jakhar, 2002); (b) Geological setting of the Newania carbonatite complex (after Tantkar, 2019).

near Udaipur, respectively (Fig. 1a; Gupta, 1934; Heron, 1953; Fareeduddin and Banerjee, 2020). The older group occurs south of Nathdwara and is Palaeoarchean-to-early Palaeoproterozoic, forming the basement for Aravalli and Delhi supergroups (Gupta, 1934; Ahmad *et al.*, 2020), whereas the younger group, lying north of Nathdwara is dominantly late Proterozoic in age (~1.7 Ga; Fareeduddin and Kroner, 1998; Buick *et al.*, 2006; Dharma Rao *et al.*, 2011). The older complex is essentially undeformed and consists of granitic, metabasic, metasedimentary and ultrabasic rocks. The granites include orthogneisses and granitoids. The granitoids are younger than orthogneisses and are Neoarchean-to-Palaeoarchean in age. These intrude the older rocks in and around Gingla, Ahar River and Berach (Ahmad *et al.*, 2020). The Untala granite is one such undeformed granitoid body located near Untala (Vallabhnaagar, Rajasthan). This is a lens-shaped intrusion which covers an area of ~300 km² and is composed of grey diorite-tonalite-trondhjemite and pink-to-grey granite, gradational into granodiorite (Roy and Jakhar, 2002; Ramakrishnan and Vaidyanandhan, 2010; GSI, 2011).

Local Geology

The Newania carbonatite complex (24°39'2.98"N, 74°03'32.75"E) is located NE of Newania village, ~40 km from Udaipur city in Rajasthan. It is ~3 km in length, forming a NW–SE trending plutonic body which has intruded the Untala granite (Fig. 1b; Viladkar, 1980; Viladkar and Pawaskar, 1989; Ray *et al.*, 2013). The complex has been emplaced within structurally weak zones in the Aravalli rift (Viladkar and Wimmenauer, 1986). Small-scale brecciation at the contact between carbonatite and country rock is present (Viladkar, 1980). Undersaturated alkaline silicate rocks are not present in the complex or in the surrounding areas (Viladkar, 1980; Viladkar and Wimmenauer, 1986). The complex is surrounded by a fenitised aureole, extending up to a distance of 75 m from the contact between carbonatite and country rock (Viladkar and Wimmenauer, 1986; Viladkar and Pawaskar, 1989).

The Newania carbonatite complex is a plutonic dolomite carbonatite with minor ferrocarbonatite, which occurs as bands, dykes and veins in the former. A laterite cap covers the complex. The weathered exposures of dolomite carbonatite are mostly brown whereas fresh outcrops are greyish-white in colour. In hand specimens, these are coarse-to-medium-grained rocks, composed dominantly of carbonate crystals, ranging in size up to 3 mm in diameter. Melanocratic bands composed of apatite, amphibole and magnetite are common. Apatite lenses up to a few cm in length are present. Ferrocarbonatite is dark maroon in colour and is exposed mainly in the north-western region of the complex. Bands and lenses of apatite, ranging from a few millimetres to metres are present in ferrocarbonatite. Laterite exposures are mostly present at the margins of the complex and have a sharp contact with the underlying carbonatite. Fresh exposures of laterite are yellowish brown in colour with visible crystals of mica. Fenite exposures around the complex are obscured by agricultural fields. A few exposures can be seen within the north-western region of the complex. These are fine-to-coarse, green-to-off-white, massive-to-banded rocks in which large crystals of amphibole, mica and feldspar can be recognised.

The Newania carbonatite complex is Proterozoic in age, although various ages have been determined by different investigations. The earliest attempts by Deans and Powell (1968) gave a K-Ar age of 959 Ma for alkali amphibole in fenite. Schleicher *et al.* (1997) and Sorokhtina *et al.* (2022) have reported the oldest emplacement ages of ~2.1–2.3 Ga for the dolomite carbonatite. Ankerite carbonatite, here termed ferrocarbonatite, is considered to have an age between ~1.4 to 1.5 Ga (Schleicher *et al.*, 1997; Ray *et al.*, 2013). Younger ages ranging between 900 and 950 Ma are reported by Gruau *et al.* (1995) and Ray *et al.* (2013) and are considered to represent a high-temperature metamorphic event.

Analytical techniques

Petrographic studies of polished sections of dolomite carbonatite were carried out using an Olympus CX31 optical microscope at

Panjab University, Chandigarh and Hitachi S-3400 N Scanning Electron Microscope at the CSIR-National Geophysical Research Institute, Hyderabad, India. Compositions of carbonate, silicate, phosphate and oxide minerals were determined using a five-channel CAMECA SX-5 electron probe micro-analyser (EPMA), installed at the Department of Earth Sciences, Indian Institute of Technology, Bombay. Details of the calibration settings of the instrument and standards used are given in Supplementary Table S1. The average lower limit of detection (LLD) for analysed elements is given in the tables in the Mineral composition section.

Petrography

Dolomite carbonatite is a coarse-to-fine-grained, equigranular rock, consisting dominantly of ferroan dolomite. Accessory minerals include apatite, amphibole, magnetite, graphite, monazite, pyrochlore and columbite which display intra-intrusion modal variations (Fig. 2a–h). Ferroan dolomite occurs as coarse-to-medium-grained subhedral crystals with a mosaic texture (Fig. 2a). Signatures of deformation are evident which include well-defined triple-junctions and thick twin lamellae. Grain boundaries are serrated and show bulging and creep (Fig. 2c,f,g). Magnesian siderite occurs as fine-to-medium-grained subhedral crystals, found at interstices of ferroan dolomite grains. These are found in textural equilibrium with apatite (Fig. 2e).

Apatite is the most abundant non-carbonate phase, occurring as fine-to-medium-grained, subhedral-to-anhedral, finely fractured crystals. Two textural varieties of apatite are recognised, designated as Ap-1 and Ap-2. Variety Ap-1 occurs in monomineralic layers of equant crystals with triple junctions and mosaic texture (Fig. 2b). The apatite grains at boundaries of such layers have abraded margins. Variety Ap-2 occurs as discrete crystals or clusters of elliptical/pill-shaped crystals (Fig. 2c–e). Monazite is typically associated with apatite, occurring as fine-grained, subhedral-to-anhedral crystals, commonly penetrating the apatite grains. Two textural varieties of monazite are present, designated as Mnz-1 and Mnz-2. Variety Mnz-1 is associated with Ap-1 as subhedral-to-anhedral inclusions within apatite bands (Fig. 2b). These also occur as aggregates of >3 elliptical crystals, in direct contact with apatite. Mnz-2 occurs as discrete crystals, associated with Ap-2 (Fig. 2d). These are porous and have similar crystal habit as Ap-2. Patchy zoning is evident in a few monazite crystals. These are anhedral coarse-grained (up to 1000 µm in diameter) crystals. High and low AZ (average atomic number) regions are difficult to demarcate in back-scattered electron images; however, false-colour X-ray element-distribution maps show a core, enveloped with an intermediate zone and outermost rim (Fig. 3a–d). Both Mnz-1 and Mnz-2 are exclusively associated with Ap-1 and Ap-2, respectively.

Two amphibole types have been identified and designated as Amp-1 and Amp-2. Type Amp-1 occurs as medium-to-fine-grained, prismatic crystals generally confined to clusters showing pleochroism from greenish blue-to-light lavender blue-to-light bluish grey (Fig. 2f). The Amp-2 type forms fine-grained prismatic-to-bladed individual crystals and is pleochroic from light brown-to-nearly colourless (Fig. 2g). Both amphibole populations are present at carbonate interstices and are an early crystallised phase relative to the surrounding carbonates. Very fine-grained (>50 µm) inclusions of graphite are present within amphibole, apatite and ferroan dolomite grains.

Columbite and pyrochlore are the two Nb-bearing phases present. They have a wide variation in modal abundance,

occasionally reaching up to 5 vol.%. Two textural varieties of columbite are identified: (1) Clb-1, which forms fine-grained (up to 150 µm), subhedral crystals with oval margins; intergrown with pyrochlore, forming composite grains; baryte is also present at crystal margins; and (2) Clb-2, occurring as fine-grained (up to 30 µm) subhedral-to-euhedral crystals (Fig. 2h). Both columbite varieties are commonly found at ferroan dolomite interstices. Magnetite are rare fine-grained euhedral-to-subhedral crystals, occurring as either individual grains or in layers with amphiboles.

Mineral compositions

Carbonates

Representative compositions of carbonates are given in Table 1. These are ferroan dolomite, containing 10.7–12.8 wt.% FeO, 13.9–15.4 wt.% MgO and 27.4–29.8 wt.% CaO. The contents of MnO and SrO vary up to 0.9 wt.%. These compositions partially overlap with carbonate compositions determined in earlier studies of the Newania carbonatite (Fig. 4a–c; Viladkar and Wimmenauer, 1986; Doroshkevich *et al.*, 2010a; Ray *et al.*, 2013). They display compositional evolution by increasing Fe and decreasing Mg contents, in common with magmatic dolomite-to-ferroan dolomite in other carbonatite complexes (Fig. 4a–c; Viladkar and Subramanian, 1995; Doroshkevich *et al.*, 2007, 2010b; Chakhmouradian *et al.*, 2009, 2016; Mitchell and Smith, 2017; Rampilova *et al.*, 2021; Boukirou *et al.*, 2022).

Magnesian siderite displays restricted compositions in comparison with previously reported compositions from Newania carbonatites (Fig. 4a–c; Buckley and Woolley, 1990; Woolley and Buckley, 1993; Doroshkevich *et al.*, 2010a; Ray *et al.*, 2013). These are characterised by 34.5–35.1 wt.% FeO, 19.2–19.5 wt.% MgO, 1.5–1.6 wt.% MnO and 0.8–0.9 wt.% CaO contents. These magnesian siderite fall well within the compositional ranges of magnesite–siderite solid solutions found in the Gleibat Lafhouda carbonatite, Morocco (Boukirou *et al.*, 2022) and Ashram Zone carbonatite, Québec, Canada (Mitchell and Smith, 2017; Fig. 4a–c).

Apatite

Compositions of Newania apatite are given in Table 2 which shows that they are fluorapatite, containing >3.2 wt.% F. Compositional zoning is absent. Ap-1 contains lower Sr (0.4–0.8 wt.% SrO) and light REE (0.2–1.0 wt.% Σ LREE₂O₃) contents than Ap-2 (1.3–2.0 wt.% SrO; 0.9–1.5 wt.% Σ LREE₂O₃). The contents of Na, Si and Fe are low (<0.4 wt.%). Newania apatite display compositional evolution from Ap-1 to Ap-2 indicated by Sr, Na and LREE enrichment and simultaneous Ca depletion (Fig. 5a,b).

Three major substitution mechanisms are evident in Newania apatite: (1) $\text{Si}^{4+} + \text{REE}^{3+} \leftrightarrow \text{Ca}^{2+} + \text{P}^{5+}$; (2) $\text{Na}^+ + \text{REE}^{3+} \leftrightarrow 2\text{Ca}^{2+}$; and (3) $\text{Sr}^{2+} \leftrightarrow \text{Ca}^{2+}$ (Fig. 5a–c). Substitution mechanism (1) or britholite-type is shown by both Ap-1 and Ap-2 (Fig. 5a). Substitution mechanism (2) or belovite-type substitution is more pronounced in Ap-2 than Ap-1 apatite (Fig. 5b). These apatites display a positive correlation of 1:1 between Na and REE (Fig. 5d). Substitution of Ca for Sr varies from 1:1 to 2:1 ratio for Ap-1 to Ap-2 (Fig. 5c). Previously published data for Newania apatite (Viladkar and Wimmenauer, 1986; Doroshkevich *et al.*, 2010a; Ray *et al.*, 2013) are similar to Ap-2 and display similar substitution trends whereas Ap-1 compositions have not been reported previously (Fig. 5a–d). The substitution mechanisms shown by Newania apatite are similar to those of other carbonatite apatites

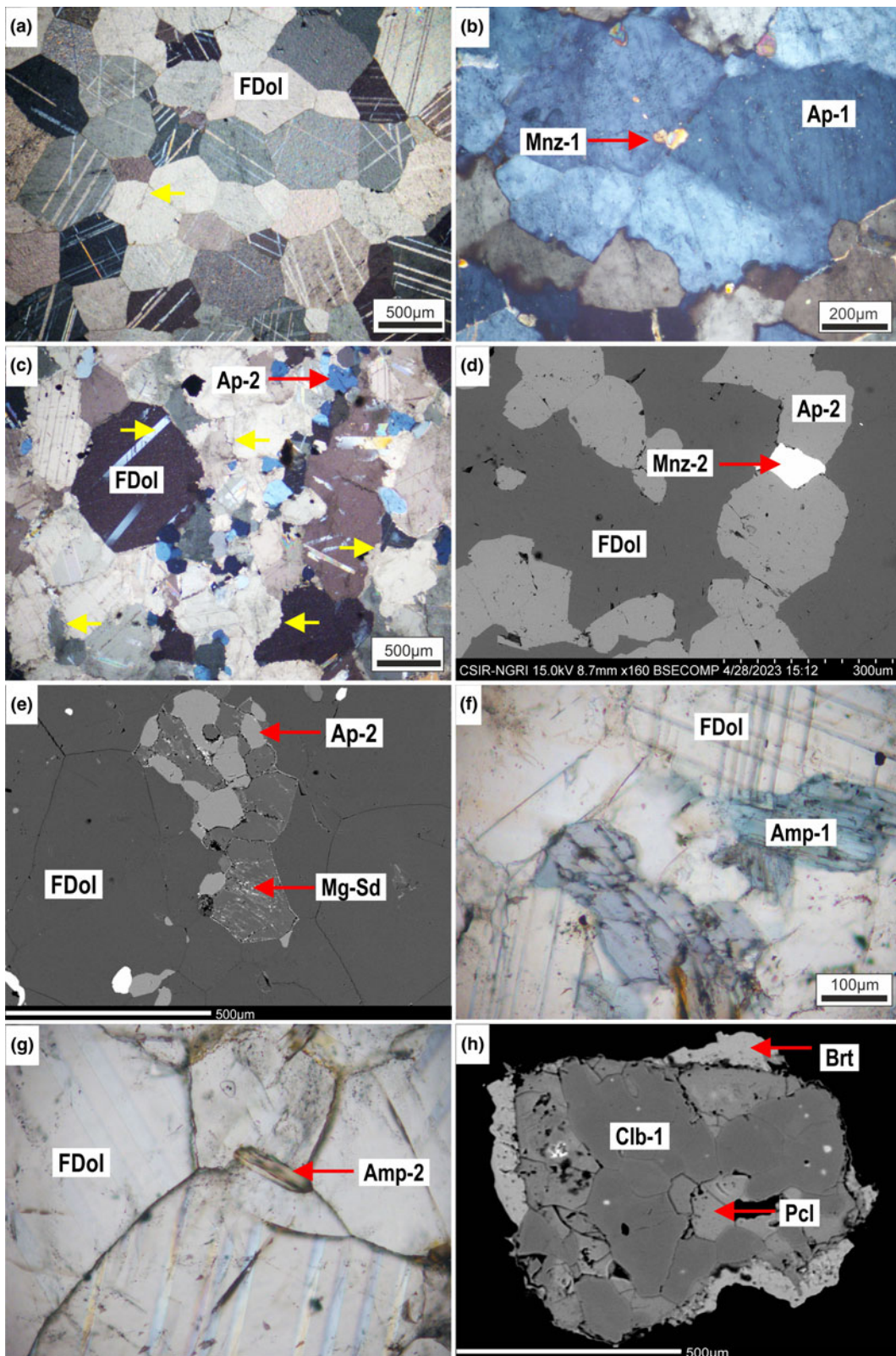


Figure 2. Photomicrographs of dolomite carbonatite in the Newania carbonatite complex, illustrating (a) crossed polars (xpl), ferroan dolomite set in mosaic fabric with triple junctions; (b) xpl, Ap-1 band and Mnz-1 crystals at grain boundaries, penetrating into the former; fractures and wavy extinction are visible; (c,d) xpl and back-scattered electron (BSE) image, respectively, textural relationships among ferroan dolomite, apatite and monazite; carbonate crystals show evidence of deformation; (e) BSE image, magnesian siderite in cluster with Ap-2 showing vein-like network; (f) plane polarised light (ppl), Amp-1 crystals at carbonate interstices; (g) ppl, single Amp-2 grain at interstices of ferroan dolomite; (h) BSE image, columbite–pyrochlore composite grain with baryte at boundary. Yellow arrows in (a) and (c) indicate signatures of deformation. (Abbreviations – Amp: amphibole, Ap: apatite, Brt: baryte, Clb: columbite, FDol: ferroan dolomite, Mg-Sd: magnesian siderite, Mnz: monazite, Pcl: pyrochlore).

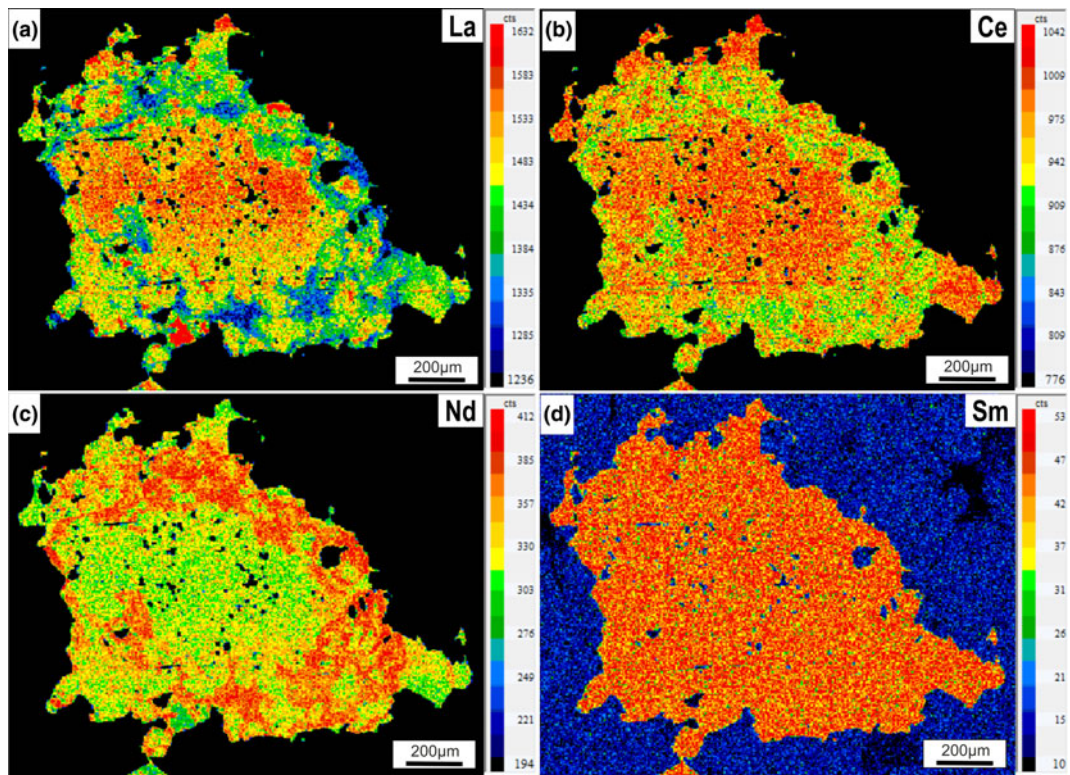


Figure 3. False colour X-ray element-distribution map showing variation in (a) La; (b) Ce; (c) Nd; and (d) Sm contents in a zoned monazite in dolomite carbonatite.

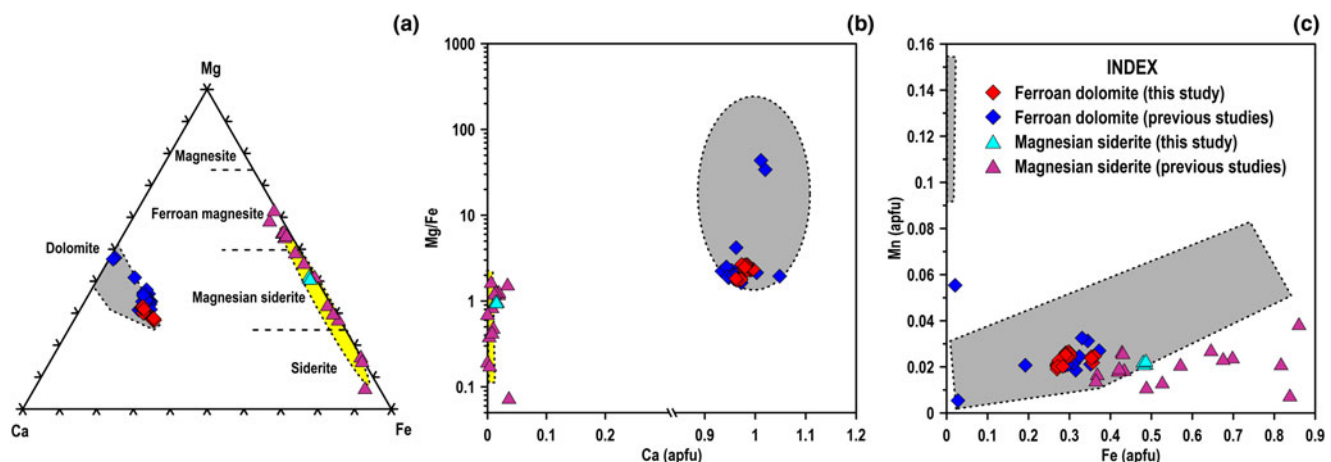


Figure 4. Compositional variation of carbonates in the Newania carbonatites. (a) Ca-Mg-Fe plot (after Mitchell and Smith, 2017); (b) Mg/Fe vs. Ca (apfu); (c) Mn vs. Fe (apfu). Grey field: dolomite–ferroan dolomite compositions in global carbonatites; yellow field: magnesite–siderite carbonate compositions in global carbonatites; data for compositional fields of carbonates are taken from Viladkar and Subramanian (1995), Doroshkevich *et al.* (2007, 2010b), Chakhmouradian *et al.* (2009, 2016), Mitchell and Smith (2017), Rampilova *et al.* (2021), Boukirou *et al.* (2022); previously published data for Newania carbonates are from Viladkar and Wimmenauer (1986), Buckley and Woolley (1990), Woolley and Buckley (1993), Doroshkevich *et al.* (2010a), Ray *et al.* (2013).

(Fig. 5a–c; Viladkar and Wimmenauer, 1992; Viladkar and Subramanian, 1995; Doroshkevich *et al.*, 2007, 2010b; Melluso *et al.*, 2010; Burtseva *et al.*, 2013; Sadiq *et al.*, 2014; Guarino *et al.*, 2017; Fosu *et al.*, 2019; Rampilova *et al.*, 2021; Boukirou *et al.*, 2022).

Monazite

The compositions of zonation-free and zoned monazite are given in Table 3. The two textural varieties (Mnz-1 and Mnz-2) show significant compositional contrast in LREE (La, Pr, Nd and Sm)

contents except for Ce which is the dominant REE in both the varieties, ranging from 31.3 to 35.4 wt.% Ce_2O_3 (Fig. 6a,b). Mnz-1 are characterised by lower La (13.6–17.4 wt.% La_2O_3) and higher Pr (3.8–4.5 wt.% Pr_2O_3), Nd (11.0–15.4 wt.% Nd_2O_3) and Sm (1.1–2.2 wt.% Sm_2O_3) contents as compared to Mnz-2 (24.3–25.4 wt.% La_2O_3 ; 2.6–3.0 wt.% Pr_2O_3 ; 6.6–7.9 wt.% Nd_2O_3 ; 0.4–0.5 wt.% Sm_2O_3). Uranium is below the detection limit and Th content reaches up to 1.2 wt.% in Mnz-2.

False colour X-ray elemental maps of zoned monazites show a La–Ce-rich core, enveloped by a discontinuous La–Ce-poor

Table 1. Compositions of carbonates in dolomite carbonatite.

| Oxide (wt.%) | LLD (wt.%) | Ferroan dolomite | | | | | | | | | | | | |
|--|---------------|------------------|-------|-------|-------|-------|-------|-------|-------|-------|-------|-------|-------|-------|
| | | 1 | 2 | 3 | 4 | 5 | 6 | 7 | 8 | 9 | 10 | 11 | 12 | 13 |
| FeO | 0.09 | 10.65 | 10.51 | 10.72 | 10.88 | 10.83 | 10.67 | 10.41 | 10.37 | 12.48 | 12.69 | 12.52 | 12.38 | 12.78 |
| MnO | 0.08 | 0.93 | 0.93 | 0.95 | 0.88 | 0.92 | 0.87 | 0.91 | 0.89 | 0.84 | 0.85 | 0.76 | 0.84 | 0.86 |
| MgO | 0.03 | 13.75 | 13.73 | 14.00 | 13.91 | 13.89 | 13.87 | 13.72 | 13.64 | 12.68 | 12.47 | 12.5 | 12.45 | 12.55 |
| CaO | 0.06 | 27.77 | 28.03 | 27.41 | 27.52 | 27.67 | 27.94 | 27.79 | 27.77 | 26.69 | 26.79 | 26.49 | 26.62 | 26.57 |
| SrO | 0.08 | 0.28 | 0.40 | 0.20 | 0.21 | 0.14 | 0.17 | 0.32 | 0.38 | 0.82 | 0.86 | 0.93 | 0.90 | 0.90 |
| Total | | 53.38 | 53.59 | 53.28 | 53.38 | 53.44 | 53.51 | 53.14 | 53.04 | 53.51 | 53.66 | 53.18 | 53.19 | 53.65 |
| Structural formula calculated on the basis of 2 cations for ferroan dolomite and 1 cation for magnesian siderite | | | | | | | | | | | | | | |
| Fe | | 0.296 | 0.291 | 0.298 | 0.302 | 0.301 | 0.296 | 0.291 | 0.290 | 0.353 | 0.359 | 0.357 | 0.353 | 0.362 |
| Mn | | 0.026 | 0.026 | 0.027 | 0.025 | 0.026 | 0.024 | 0.026 | 0.025 | 0.024 | 0.024 | 0.022 | 0.024 | 0.025 |
| Mg | | 0.682 | 0.679 | 0.694 | 0.689 | 0.687 | 0.685 | 0.683 | 0.681 | 0.639 | 0.629 | 0.635 | 0.633 | 0.633 |
| Ca | | 0.990 | 0.996 | 0.977 | 0.980 | 0.984 | 0.992 | 0.994 | 0.996 | 0.967 | 0.971 | 0.968 | 0.972 | 0.963 |
| Sr | | 0.005 | 0.008 | 0.004 | 0.004 | 0.003 | 0.003 | 0.006 | 0.007 | 0.016 | 0.017 | 0.018 | 0.018 | 0.018 |
| Total | | 2.000 | 2.000 | 2.000 | 2.000 | 2.000 | 2.000 | 2.000 | 2.000 | 2.000 | 2.000 | 2.000 | 2.000 | 2.000 |
| Ferroan dolomite | | | | | | | | | | | | | | |
| | 14 | 15 | 16 | 17 | 18 | 19 | 20 | 21 | | 22 | 23 | 24 | 25 | |
| FeO | 12.47 | 9.68 | 9.80 | 9.90 | 9.65 | 9.85 | 9.85 | 11.06 | | 35.08 | 34.82 | 34.49 | 35.15 | |
| MnO | 0.83 | 0.73 | 0.77 | 0.76 | 0.67 | 0.81 | 0.73 | 0.78 | | 1.53 | 1.52 | 1.60 | 1.64 | |
| MgO | 12.78 | 14.41 | 14.51 | 14.57 | 14.42 | 14.36 | 14.74 | 15.41 | | 19.21 | 19.43 | 19.52 | 19.27 | |
| CaO | 26.48 | 27.73 | 27.87 | 27.75 | 27.42 | 27.53 | 27.58 | 29.79 | | 0.85 | 0.93 | 0.79 | 0.86 | |
| SrO | 0.79 | 0.77 | 0.75 | 0.69 | 0.61 | 0.69 | 0.66 | 0.64 | | bdl | bdl | bdl | bdl | |
| Total | 53.34 | 53.30 | 53.70 | 53.67 | 52.76 | 53.23 | 53.55 | 57.67 | | 56.66 | 56.70 | 56.38 | 56.91 | |
| Structural formula calculated on the basis of 2 cations for ferroan dolomite and 1 cation for magnesian siderite | | | | | | | | | | | | | | |
| Fe | | 0.353 | 0.268 | 0.270 | 0.272 | 0.270 | 0.273 | 0.271 | 0.284 | | 0.487 | 0.482 | 0.480 | 0.486 |
| Mn | | 0.024 | 0.020 | 0.021 | 0.021 | 0.019 | 0.023 | 0.020 | 0.020 | | 0.022 | 0.021 | 0.022 | 0.023 |
| Mg | | 0.646 | 0.712 | 0.712 | 0.715 | 0.718 | 0.711 | 0.723 | 0.705 | | 0.476 | 0.480 | 0.484 | 0.475 |
| Ca | | 0.962 | 0.985 | 0.983 | 0.979 | 0.982 | 0.980 | 0.973 | 0.980 | | 0.015 | 0.016 | 0.014 | 0.015 |
| Sr | | 0.016 | 0.015 | 0.014 | 0.013 | 0.012 | 0.013 | 0.013 | 0.011 | | - | - | - | - |
| Total | | 2.000 | 2.000 | 2.000 | 2.000 | 2.000 | 2.000 | 2.000 | | 1.000 | 1.000 | 1.000 | 1.000 | |

LLD – lower limit of detection; bdl – below detection limit.

and Nd-rich intermediate zone; an outermost partial rim compositionally resembling the core is also present (Fig. 3). Compositionally, these overlap with unzoned Mnz-1. The core contains lower La (14.9–15.0 wt.% La_2O_3) and Ce (31.9–32.2 wt.% Ce_2O_3) and higher Pr (4.2–4.3 wt.% Pr_2O_3), Nd (15.6–15.8 wt.% Nd_2O_3) and Sm (1.8–2.1 wt.% Sm_2O_3) than intermediate zone (16.5–17.3 wt.% La_2O_3 , 33.1–34.2 wt.% Ce_2O_3 , 3.8–4.2 wt.% Pr_2O_3 , 12.5–13.7 wt.% Nd_2O_3 and 1.3–1.5 wt.% Sm_2O_3) and outermost rim (17.2 wt.% La_2O_3 , 33.1 wt.% Ce_2O_3 , 4.2 wt.% Pr_2O_3 , 13.4 wt.% Nd_2O_3 and 1.4 wt.% Sm_2O_3).

Newania monazite fall well within the compositional field of worldwide carbonatite monazites (Fig. 6a; Chen *et al.*, 2017) and are classified as monazite-(Ce). Compositional trends of La enrichment and depletion in Pr, Nd and Sm contents are evident from Mnz-1 to Mnz-2. Cerium displays two distinct compositional evolutionary trends where Ce content increases in Mnz-1 and decreases in Mnz-2 as La content increases (Fig. 6b). The two substitution mechanisms shown by Newania monazite are huttonite $\{(\text{Th},\text{U})^{4+} + \text{Si}^{4+} \leftrightarrow \Sigma\text{REE}^{3+} + \text{P}^{5+}\}$ and brabantite, now called cheralite $\{(\text{Th},\text{U})^{4+} + \text{Ca}^{2+} \leftrightarrow 2\Sigma\text{REE}^{3+}\}$; the former being shown by Mnz-1 with $\Sigma\text{REE}^{3+} + \text{P}^{5+} > 1.994$ atoms per formula unit (apfu), whereas the latter substitution is shown by Mnz-2 and Mnz-1 with $\Sigma\text{REE}^{3+} + \text{P}^{5+} < 1.994$ apfu (Fig. 6c–d). Similar composition and substitution trends are displayed by other carbonatite monazites (Fig. 6b–d; Burtseva *et al.*, 2013; Basu and Bhattacharya, 2014; Sadiq *et al.*, 2014; Dalsin *et al.*, 2015; Trofanenko *et al.*, 2016; Chen *et al.*, 2017 and references cited therein; Rampilova *et al.*, 2021).

Amphibole

Both types of Newania amphibole display restricted compositional variation (Table 4). Amp-1 is characterised by 12.2–12.7 wt.% total FeO, 15.8–16.6 wt.% MgO and 4.1–5.1 wt.% CaO contents. The contents of Na and K range from 5.3–6.3 wt.% and 0.5–0.6 wt.%, respectively. These contain up to 0.4 wt.% Al_2O_3 , 0.1 wt.% TiO_2 and 0.2 wt.% MnO. Compositionally, Amp-1 belongs to the sodium-calcium subgroup of the amphibole supergroup and is ferri-winchite (Fig. 7a). Amp-2 contains 26.3–26.4 wt.% total FeO, 14.5–14.6 wt.% MgO and 0.8–1.1 wt. % Na_2O contents. The content of Ca, Mn and F varies from 0.4 to 0.6 wt.%. Potassium, Al and Ti contents reach up to 0.1 wt.%. Amp-2 belongs to the magnesium-iron-manganese subgroup amphiboles and is compositionally equivalent to cummingtonite (Fig. 7b).

Previously published amphibole compositions of Newania carbonatites when recalculated using the spreadsheet of Locock (2014) suggest the presence of magnesio-afvedsonite, magnesio-riebeckite and ferri-katophorite (Vladkar and Wimmenauer, 1986; Doroshkevich *et al.*, 2010a; Ray *et al.*, 2013). The compositions display an evolutionary trend from ferri-katophorite to magnesio-afvedsonite and magnesio-riebeckite, which is similar to the evolution of other carbonatite amphiboles (Fig. 8a; Samoylov, 1977; Martin, 2007; Reguir *et al.*, 2012). The amphibole compositions obtained in this investigation differ markedly from the earlier published compositions (Fig. 8a,b), although similar amphiboles have been reported previously from a few carbonatite occurrences i.e. Veseloe, North Transbaikalia, Russia

Table 2. Compositions of Newania apatite.

| Oxide (wt.%) | LLD (wt.%) | Ap-1 | | | | | | | | | | Ap-2 | | | | | | | | | |
|---|---------------|--------|--------|--------|--------|--------|--------|--------|--------|--------|--------|--------|--------|--------|--------|--------|--------|--------|--------|--------|--------|
| | | 1 | 2 | 3 | 4 | 5 | 6 | 7 | 8 | 9 | 10 | 11 | 12 | 13 | 14 | 15 | 16 | 17 | 18 | 19 | 20 |
| P ₂ O ₅ | 0.06 | 41.41 | 41.99 | 41.96 | 42.23 | 42.06 | 41.37 | 40.91 | 41.07 | 41.43 | 41.46 | 41.10 | 41.50 | 41.98 | 41.41 | 41.51 | 41.31 | 41.59 | 41.54 | 41.02 | 41.18 |
| SiO ₂ | 0.02 | 0.04 | 0.04 | 0.12 | 0.05 | 0.03 | 0.35 | bdl | 0.04 | bdl | 0.02 | bdl | bdl | bdl | bdl | 0.03 | 0.03 | bdl | bdl | 0.04 | 0.04 |
| FeO* | 0.09 | 0.10 | bdl | 0.11 | 0.13 | 0.12 | bdl | 0.09 | bdl | bdl | bdl | bdl | bdl | 0.11 | 0.14 | bdl | 0.19 | 0.09 | 0.19 | 0.10 | 0.29 |
| CaO | 0.05 | 55.39 | 56.27 | 55.35 | 54.64 | 55.21 | 54.10 | 54.45 | 53.95 | 53.25 | 53.35 | 53.77 | 53.95 | 53.83 | 53.58 | 53.55 | 52.85 | 53.63 | 53.32 | 53.51 | 53.78 |
| SrO | 0.10 | 0.43 | 0.58 | 0.59 | 0.60 | 0.54 | 0.70 | 0.80 | 0.75 | 1.31 | 1.38 | 1.44 | 1.54 | 1.45 | 1.32 | 2.00 | 1.85 | 1.96 | 1.94 | 2.01 | 1.93 |
| Na ₂ O | 0.04 | 0.08 | 0.08 | 0.28 | 0.06 | bdl | 0.05 | 0.09 | 0.06 | 0.24 | 0.18 | 0.18 | 0.19 | 0.21 | 0.23 | 0.23 | 0.20 | 0.25 | 0.21 | 0.25 | 0.18 |
| La ₂ O ₃ | 0.08 | bdl | 0.11 | bdl | bdl | bdl | bdl | bdl | bdl | 0.19 | 0.16 | 0.14 | 0.16 | 0.18 | 0.15 | 0.21 | 0.20 | 0.23 | 0.20 | 0.19 | 0.20 |
| Ce ₂ O ₃ | 0.22 | 0.18 | 0.14 | 0.25 | 0.17 | 0.10 | 0.16 | 0.16 | bdl | 0.46 | 0.43 | 0.43 | 0.47 | 0.44 | 0.42 | 0.51 | 0.52 | 0.45 | 0.47 | 0.52 | 0.41 |
| Pr ₂ O ₃ | 0.22 | 0.23 | bdl | 0.33 | 0.28 | 0.26 | bdl | 0.38 | 0.30 | bdl | 0.26 | 0.33 | 0.27 | bdl | bdl | 0.30 | 0.31 | 0.24 | bdl | 0.24 | 0.25 |
| Nd ₂ O ₃ | 0.24 | bdl | bdl | 0.42 | bdl | bdl | bdl | bdl | 0.32 | 0.26 | 0.37 | 0.40 | 0.29 | 0.28 | 0.40 | 0.46 | 0.40 | 0.39 | 0.39 | 0.32 | |
| F | 0.17 | 3.97 | 3.77 | 3.88 | 4.11 | 4.95 | 4.49 | 3.48 | 4.99 | 3.96 | 3.94 | 6.41 | 4.44 | 4.82 | 3.98 | 3.31 | 4.45 | 3.61 | 3.22 | 3.36 | 3.78 |
| O=F | | 1.67 | 1.59 | 1.63 | 1.73 | 2.08 | 1.89 | 1.46 | 2.10 | 1.67 | 1.66 | 2.70 | 1.87 | 2.03 | 1.68 | 1.39 | 1.87 | 1.52 | 1.36 | 1.41 | 1.59 |
| Total | | 101.82 | 102.97 | 103.29 | 102.27 | 103.25 | 101.23 | 100.37 | 101.17 | 101.16 | 101.44 | 104.17 | 102.93 | 103.32 | 101.52 | 102.05 | 102.36 | 102.44 | 101.48 | 101.61 | 102.37 |
| Corrected total | | 100.15 | 101.39 | 101.66 | 100.53 | 101.17 | 99.33 | 98.91 | 99.06 | 99.49 | 99.78 | 101.47 | 101.06 | 101.29 | 99.84 | 100.66 | 100.49 | 100.92 | 100.12 | 100.20 | 100.78 |
| ΣLREE | | 0.41 | 0.25 | 1.00 | 0.45 | 0.36 | 0.16 | 0.54 | 0.30 | 0.97 | 1.11 | 1.27 | 1.30 | 0.92 | 0.85 | 1.42 | 1.49 | 1.32 | 1.06 | 1.33 | 1.18 |
| Structural formula calculated on the basis of 8 cations | | | | | | | | | | | | | | | | | | | | | |
| P | | 2.950 | 2.948 | 2.952 | 3.008 | 2.988 | 2.984 | 2.951 | 2.982 | 2.994 | 2.992 | 2.960 | 2.969 | 2.996 | 2.980 | 2.969 | 2.983 | 2.970 | 2.982 | 2.946 | 2.946 |
| Si | | 0.003 | 0.003 | 0.010 | 0.004 | 0.002 | 0.030 | - | 0.003 | - | 0.002 | - | - | - | - | 0.003 | 0.002 | - | - | 0.003 | 0.003 |
| Fe ^{2+*} | | 0.007 | - | 0.007 | 0.009 | 0.008 | - | 0.007 | - | - | - | - | - | 0.008 | 0.010 | - | 0.014 | 0.006 | 0.014 | 0.007 | 0.021 |
| Ca | | 4.994 | 5.000 | 4.928 | 4.926 | 4.964 | 4.938 | 4.971 | 4.958 | 4.871 | 4.873 | 4.901 | 4.884 | 4.863 | 4.880 | 4.849 | 4.830 | 4.847 | 4.843 | 4.863 | 4.869 |
| Sr | | 0.021 | 0.028 | 0.028 | 0.029 | 0.026 | 0.035 | 0.040 | 0.037 | 0.065 | 0.068 | 0.071 | 0.076 | 0.071 | 0.065 | 0.098 | 0.091 | 0.096 | 0.095 | 0.099 | 0.095 |
| Na | | 0.012 | 0.013 | 0.044 | 0.009 | - | 0.009 | 0.016 | 0.010 | 0.040 | 0.030 | 0.029 | 0.032 | 0.034 | 0.038 | 0.038 | 0.034 | 0.040 | 0.034 | 0.041 | 0.030 |
| La | | - | 0.003 | - | - | - | - | - | - | 0.006 | 0.005 | 0.004 | 0.005 | 0.006 | 0.005 | 0.007 | 0.006 | 0.007 | 0.006 | 0.006 | 0.006 |
| Ce | | 0.006 | 0.004 | 0.008 | 0.005 | 0.003 | 0.005 | 0.005 | - | 0.014 | 0.014 | 0.014 | 0.015 | 0.014 | 0.013 | 0.016 | 0.016 | 0.014 | 0.015 | 0.016 | 0.013 |
| Pr | | 0.007 | - | 0.010 | 0.008 | 0.008 | - | 0.012 | 0.009 | - | 0.008 | 0.010 | 0.008 | - | - | 0.009 | 0.010 | 0.007 | - | 0.008 | 0.008 |
| Nd | | - | - | 0.012 | - | - | - | - | 0.010 | 0.008 | 0.011 | 0.012 | 0.009 | 0.008 | 0.012 | 0.014 | 0.012 | 0.012 | 0.012 | 0.010 | |
| Total | | 8.000 | 8.000 | 8.000 | 8.000 | 8.000 | 8.000 | 8.000 | 8.000 | 8.000 | 8.000 | 8.000 | 8.000 | 8.000 | 8.000 | 8.000 | 8.000 | 8.000 | 8.000 | 8.000 | |
| F | | 1.057 | 0.988 | 1.019 | 1.094 | 1.314 | 1.210 | 0.937 | 1.354 | 1.070 | 1.061 | 1.725 | 1.186 | 1.285 | 1.071 | 0.883 | 1.200 | 0.963 | 0.864 | 0.900 | 1.009 |

FeO* – total iron expressed as FeO; Fe^{2+*} – total iron as Fe²⁺; LLD – lower limit of detection; bdl – below detection limit.

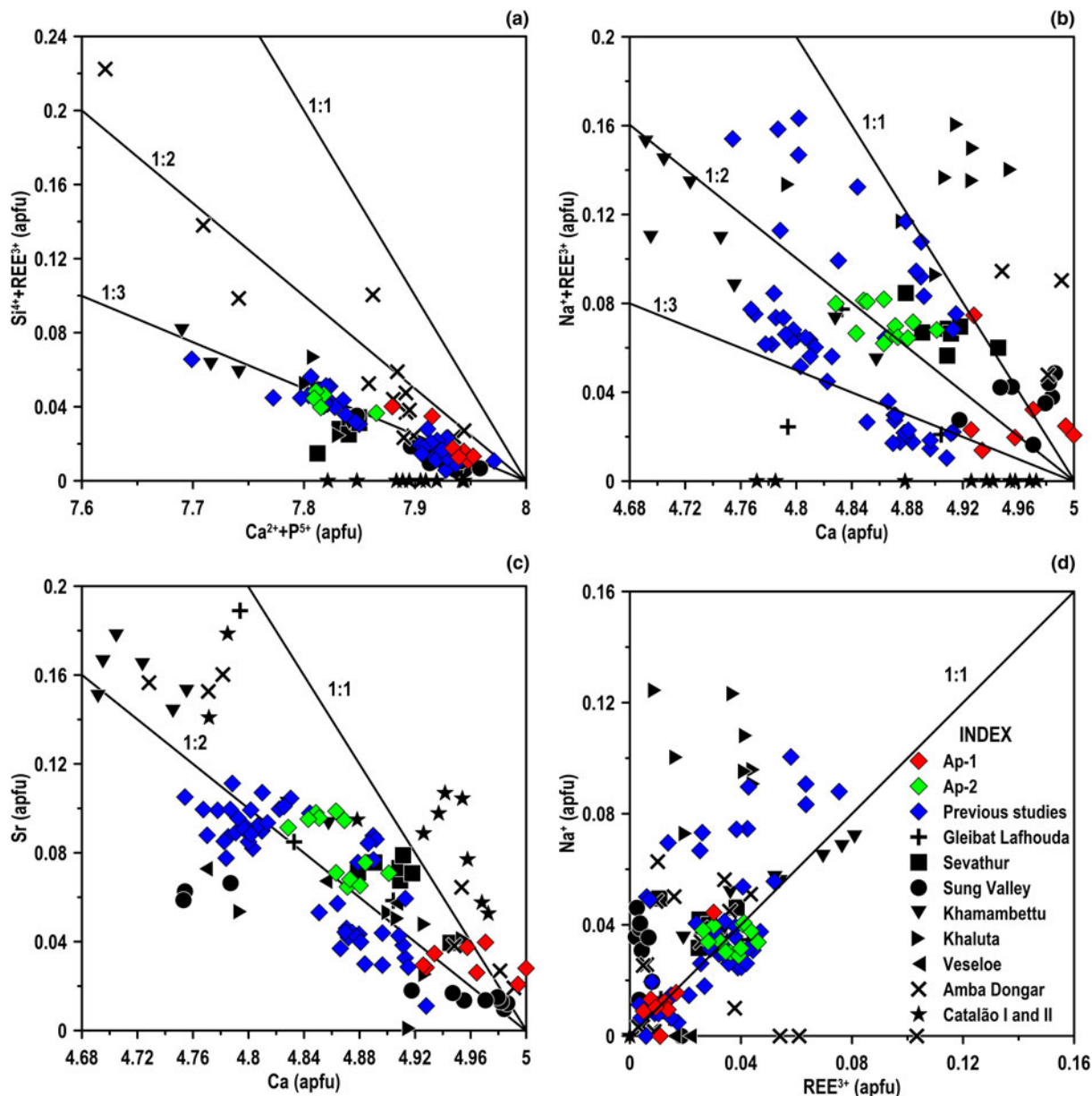


Figure 5. Compositional variation of apatite (Ap-1 and Ap-2) from the Newania carbonatite complex: (a) $\text{Si}^{4+} + \text{REE}^{3+}$ vs. $\text{Ca}^{2+} + \text{P}^{5+}$ (apfu); (b) $\text{Na}^+ + \text{REE}^{3+}$ vs. Ca^{2+} (apfu); (c) Sr^{2+} vs. Ca^{2+} (apfu); and (d) Na^+ vs. REE^{3+} (apfu). Data for carbonatitic apatite are from Viladkar and Wimmenauer (1992), Viladkar and Subramanian (1995), Doroshkevich *et al.* (2007, 2010b), Melluso *et al.* (2010), Burtseva *et al.* (2013), Sadiq *et al.* (2014), Guarino *et al.* (2017), Fosu *et al.* (2019), Rampilova *et al.* (2021), Boukirou *et al.* (2022); previously published apatite compositions for Newania are from Viladkar and Wimmenauer (1986), Doroshkevich *et al.* (2010a), Ray *et al.* (2013).

(Doroshkevich *et al.*, 2007), Fir, British Columbia, Canada (Chudy, 2014) and Huayangchuan carbonatites, Central China (Reguir *et al.*, 2012; Fig. 8a–c).

Columbite

The compositions of columbite are given in Table 5. Clb-1 contains 67.9–77.3 wt.% Nb_2O_5 , 1.6–3.4 wt.% Ta_2O_5 , 7.7–18.7 wt.% FeO and 1.0–4.1 wt.% TiO_2 . Clb-2 is characterised by similar Nb (68.4–73.9 wt.% Nb_2O_5), higher Ta (4.5–10.0 wt.% Ta_2O_5) and Fe (18.4–19.1 wt.% FeO) and lower Ti (0.3–0.8 wt.% TiO_2) contents than Clb-1. The manganese content is below the detection limit (800 ppm). Compositionally, Clb-1 and Clb-2 are iron-rich members of the columbite supergroup i.e. columbite-(Fe) (Chukanov *et al.*, 2023). Previously published columbite

compositions from Newania carbonatites resemble those of Clb-2 (Fig. 9; Viladkar *et al.*, 2017). An increase in Ta content from Clb-1 to Clb-2 is similar to the compositional evolution of columbite from Fir carbonatites (Chudy, 2014). Overall, the compositions of Newania columbite-(Fe) are similar to those found in Fir (Chudy, 2014) and Gleibat Lafhouda (Boukirou *et al.*, 2022) whereas those from Aley, British Columbia, Canada (Chakhmouradian *et al.*, 2015) and Ashram (Mitchell and Smith, 2017) are relatively depleted in Ta (Fig. 9).

Pyrochlore

The compositions of pyrochlore in the dolomite carbonatite are given in Table 6. The nomenclature used for the pyrochlore supergroup follows Atencio *et al.* (2010) and Bhattacharjee

Table 3. Compositions of Newania monazite.

| Oxides (wt.%) | LLD (wt.%) | Mnz-1 | | | | | | | | | | | | Mnz-2 | | | | | | | | | | | | | | |
|---|------------|---------|-------|-------|-------|-------|-------|--------|-------|-------|-------|-------|-------|-------|-------|-------|-------|--------|--------|------------------|--------|--------|-------|-------|--------|--------|-------|------|
| | | Unzoned | | | | | | Zoned* | | | | | | Core | | | | | | Intermediate rim | | | Outer | | | | | |
| | | 1 | 2 | 3 | 4 | 5 | 6 | 7 | 8 | 9 | 10 | 11 | 12 | 13 | 14 | 15 | 16 | 17 | 18 | 19 | 20 | 21 | 22 | 23 | 24 | 25 | 26 | |
| P ₂ O ₅ | 0.06 | 30.34 | 29.89 | 30.31 | 29.46 | 29.37 | 30.12 | 30.01 | 29.91 | 30.18 | 30.00 | 29.35 | 30.12 | 29.74 | 29.73 | 29.21 | 29.71 | 29.82 | 30.00 | 30.61 | 30.15 | 29.97 | 30.25 | 29.63 | 29.77 | 30.38 | 30.08 | |
| SiO ₂ | 0.03 | 0.12 | 0.12 | 0.08 | 0.13 | 0.11 | 0.12 | 0.10 | 0.08 | 0.06 | 0.10 | 0.10 | 0.14 | 0.07 | 0.09 | 0.12 | 0.13 | 0.11 | 0.11 | 0.08 | 0.08 | 0.10 | 0.09 | 0.09 | 0.54 | 0.18 | 0.09 | |
| CaO | 0.04 | bdl | 0.07 | 0.15 | 0.19 | 0.11 | 0.05 | 0.10 | bdl | bdl | bdl | bdl | bdl | 0.07 | 0.11 | 0.05 | 0.14 | 0.13 | |
| SrO | 0.14 | bdl | bdl | bdl | bdl | bdl | bdl | bdl | bdl | bdl | bdl | bdl | bdl | bdl | bdl | bdl | bdl | bdl | bdl | bdl | bdl | bdl | bdl | bdl | bdl | bdl | 0.16 | 0.18 |
| ThO ₂ | 0.15 | bdl | 0.18 | bdl | bdl | bdl | bdl | bdl | bdl | bdl | bdl | bdl | bdl | bdl | bdl | bdl | bdl | bdl | bdl | bdl | bdl | bdl | bdl | bdl | bdl | 0.23 | 0.54 | 1.16 |
| La ₂ O ₃ | 0.11 | 15.41 | 14.80 | 17.43 | 16.85 | 13.67 | 13.61 | 14.43 | 16.77 | 16.18 | 16.56 | 14.91 | 14.98 | 16.60 | 16.47 | 16.75 | 17.20 | 17.10 | 17.16 | 17.28 | 25.41 | 25.18 | 24.30 | 24.82 | 25.20 | 25.32 | 24.74 | |
| Ce ₂ O ₃ | 0.11 | 33.81 | 32.80 | 34.69 | 33.80 | 31.29 | 32.18 | 32.69 | 35.36 | 34.60 | 34.99 | 32.16 | 31.93 | 33.70 | 33.39 | 33.06 | 33.06 | 34.01 | 33.89 | 34.16 | 33.57 | 33.32 | 34.17 | 33.63 | 33.10 | 32.99 | 33.75 | |
| Pr ₂ O ₃ | 0.30 | 3.97 | 4.15 | 3.91 | 4.05 | 4.17 | 4.43 | 4.46 | 4.20 | 4.28 | 4.04 | 4.15 | 4.26 | 4.04 | 3.77 | 4.20 | 4.24 | 4.01 | 3.84 | 4.10 | 2.62 | 2.88 | 2.92 | 2.97 | 2.76 | 3.00 | 2.92 | |
| Nd ₂ O ₃ | 0.32 | 13.92 | 14.21 | 11.04 | 12.22 | 15.18 | 15.41 | 15.42 | 12.78 | 12.04 | 12.30 | 15.76 | 15.56 | 13.37 | 13.43 | 13.61 | 13.35 | 12.46 | 13.01 | 12.94 | 6.64 | 7.16 | 7.57 | 7.33 | 6.93 | 6.80 | 7.88 | |
| Sm ₂ O ₃ | 0.25 | 1.72 | 1.86 | 1.14 | 2.13 | 2.17 | 1.96 | 1.41 | 1.20 | 1.27 | 1.81 | 2.10 | 1.53 | 1.45 | 1.33 | 1.37 | 1.32 | 1.44 | 1.32 | 0.50 | 0.49 | 0.37 | 0.41 | 0.38 | 0.38 | 0.50 | | |
| F | 0.13 | 0.49 | 0.56 | 0.59 | 0.62 | 0.51 | 0.55 | 0.54 | 0.53 | 0.63 | 0.52 | 0.51 | 0.51 | 0.59 | 0.51 | 0.46 | 0.54 | 0.61 | 0.56 | 0.47 | 0.59 | 0.54 | 0.54 | 0.65 | 0.46 | 0.57 | 0.53 | |
| Cl | 0.08 | bdl | 0.09 | bdl | bdl | bdl | bdl | bdl | 0.09 | bdl | bdl | bdl | bdl | bdl | bdl | bdl | bdl | bdl | | |
| O=F | 0.20 | 0.24 | 0.25 | 0.26 | 0.21 | 0.23 | 0.23 | 0.22 | 0.27 | 0.22 | 0.21 | 0.21 | 0.25 | 0.22 | 0.19 | 0.23 | 0.26 | 0.24 | 0.20 | 0.25 | 0.23 | 0.23 | 0.27 | 0.19 | 0.24 | 0.22 | | |
| O=Cl | - | 0.02 | - | - | - | - | - | - | 0.02 | - | - | - | - | - | - | - | - | 0.02 | - | - | - | - | - | - | - | - | | |
| Total | 99.77 | 98.74 | 99.33 | 98.47 | 96.51 | 98.64 | 99.70 | 101.04 | 99.25 | 99.79 | 98.74 | 99.58 | 99.64 | 98.83 | 98.78 | 99.68 | 99.44 | 100.00 | 100.96 | 100.28 | 100.41 | 100.26 | 99.88 | 99.80 | 101.28 | 101.07 | | |
| Corrected total | 99.56 | 98.50 | 99.08 | 98.21 | 96.30 | 98.40 | 99.48 | 100.81 | 98.98 | 99.57 | 98.53 | 99.37 | 99.39 | 98.61 | 98.59 | 99.45 | 99.18 | 99.76 | 100.76 | 100.03 | 100.18 | 100.03 | 99.61 | 99.61 | 101.04 | 100.85 | | |
| ΣLREE | 68.82 | 67.83 | 68.21 | 68.06 | 66.42 | 67.80 | 68.96 | 70.51 | 68.29 | 69.17 | 68.79 | 68.82 | 69.24 | 68.51 | 68.95 | 69.21 | 68.90 | 69.33 | 69.80 | 68.75 | 69.02 | 69.33 | 69.15 | 68.37 | 68.47 | 69.80 | | |
| Structural formula calculated on the basis of 2 cations | | | | | | | | | | | | | | | | | | | | | | | | | | | | |
| P | 1.010 | 1.008 | 1.010 | 0.996 | 1.010 | 1.013 | 1.002 | 0.991 | 1.012 | 1.001 | 0.994 | 1.006 | 0.997 | 1.002 | 0.989 | 0.996 | 1.000 | 1.000 | 1.007 | 1.001 | 0.995 | 1.002 | 0.990 | 0.988 | 0.995 | 0.991 | | |
| Si | 0.005 | 0.005 | 0.003 | 0.005 | 0.004 | 0.005 | 0.004 | 0.003 | 0.002 | 0.004 | 0.004 | 0.006 | 0.003 | 0.003 | 0.005 | 0.005 | 0.004 | 0.004 | 0.003 | 0.003 | 0.004 | 0.004 | 0.004 | 0.021 | 0.007 | 0.004 | | |
| Ca | - | 0.003 | 0.006 | 0.008 | 0.005 | 0.002 | 0.004 | - | - | - | - | - | - | - | 0.002 | - | - | - | - | - | 0.003 | 0.005 | 0.002 | 0.006 | 0.005 | 0.015 | 0.006 | |
| Sr | - | - | - | - | - | - | - | - | - | - | - | - | - | - | - | - | - | - | - | - | - | - | - | - | 0.004 | 0.004 | | |
| Th | - | 0.002 | - | - | - | - | - | - | - | - | - | - | - | - | - | - | - | - | - | 0.006 | 0.006 | - | 0.002 | 0.005 | 0.010 | 0.002 | | |
| La | 0.223 | 0.217 | 0.253 | 0.248 | 0.205 | 0.199 | 0.210 | 0.242 | 0.236 | 0.241 | 0.220 | 0.218 | 0.243 | 0.242 | 0.247 | 0.251 | 0.250 | 0.249 | 0.248 | 0.368 | 0.364 | 0.351 | 0.361 | 0.364 | 0.361 | 0.355 | | |
| Ce | 0.487 | 0.478 | 0.500 | 0.494 | 0.465 | 0.468 | 0.472 | 0.507 | 0.501 | 0.505 | 0.471 | 0.461 | 0.489 | 0.487 | 0.484 | 0.479 | 0.493 | 0.489 | 0.486 | 0.482 | 0.478 | 0.490 | 0.486 | 0.475 | 0.467 | 0.481 | | |
| Pr | 0.057 | 0.060 | 0.056 | 0.059 | 0.062 | 0.064 | 0.064 | 0.060 | 0.062 | 0.058 | 0.060 | 0.061 | 0.058 | 0.055 | 0.061 | 0.061 | 0.058 | 0.055 | 0.058 | 0.037 | 0.041 | 0.042 | 0.043 | 0.039 | 0.042 | 0.041 | | |
| Nd | 0.195 | 0.202 | 0.155 | 0.174 | 0.220 | 0.219 | 0.217 | 0.179 | 0.170 | 0.173 | 0.225 | 0.219 | 0.189 | 0.191 | 0.194 | 0.189 | 0.176 | 0.183 | 0.180 | 0.093 | 0.100 | 0.106 | 0.103 | 0.097 | 0.094 | 0.110 | | |
| Sm | 0.023 | 0.026 | 0.015 | 0.016 | 0.030 | 0.030 | 0.027 | 0.019 | 0.016 | 0.017 | 0.025 | 0.028 | 0.021 | 0.020 | 0.018 | 0.019 | 0.018 | 0.019 | 0.018 | 0.007 | 0.005 | 0.006 | 0.005 | 0.005 | 0.007 | | | |
| Total | 2.000 | 2.000 | 2.000 | 2.000 | 2.000 | 2.000 | 2.000 | 2.000 | 2.000 | 2.000 | 2.000 | 2.000 | 2.000 | 2.000 | 2.000 | 2.000 | 2.000 | 2.000 | 2.000 | 2.000 | 2.000 | 2.000 | 2.000 | 2.000 | 2.000 | | | |
| F | 0.060 | 0.071 | 0.073 | 0.078 | 0.065 | 0.069 | 0.067 | 0.065 | 0.079 | 0.065 | 0.064 | 0.063 | 0.074 | 0.064 | 0.058 | 0.068 | 0.077 | 0.070 | 0.057 | 0.074 | 0.067 | 0.067 | 0.081 | 0.057 | 0.069 | 0.066 | | |
| Cl | - | 0.006 | - | - | - | - | - | - | 0.006 | - | - | - | - | - | - | - | 0.006 | - | - | - | - | - | - | - | - | | | |

LLD – lower limit of detection; bdl – below detection limit.

*Zoned samples: 11,12 = core; 13–18 = intermediate rim; 19 = outermost rim

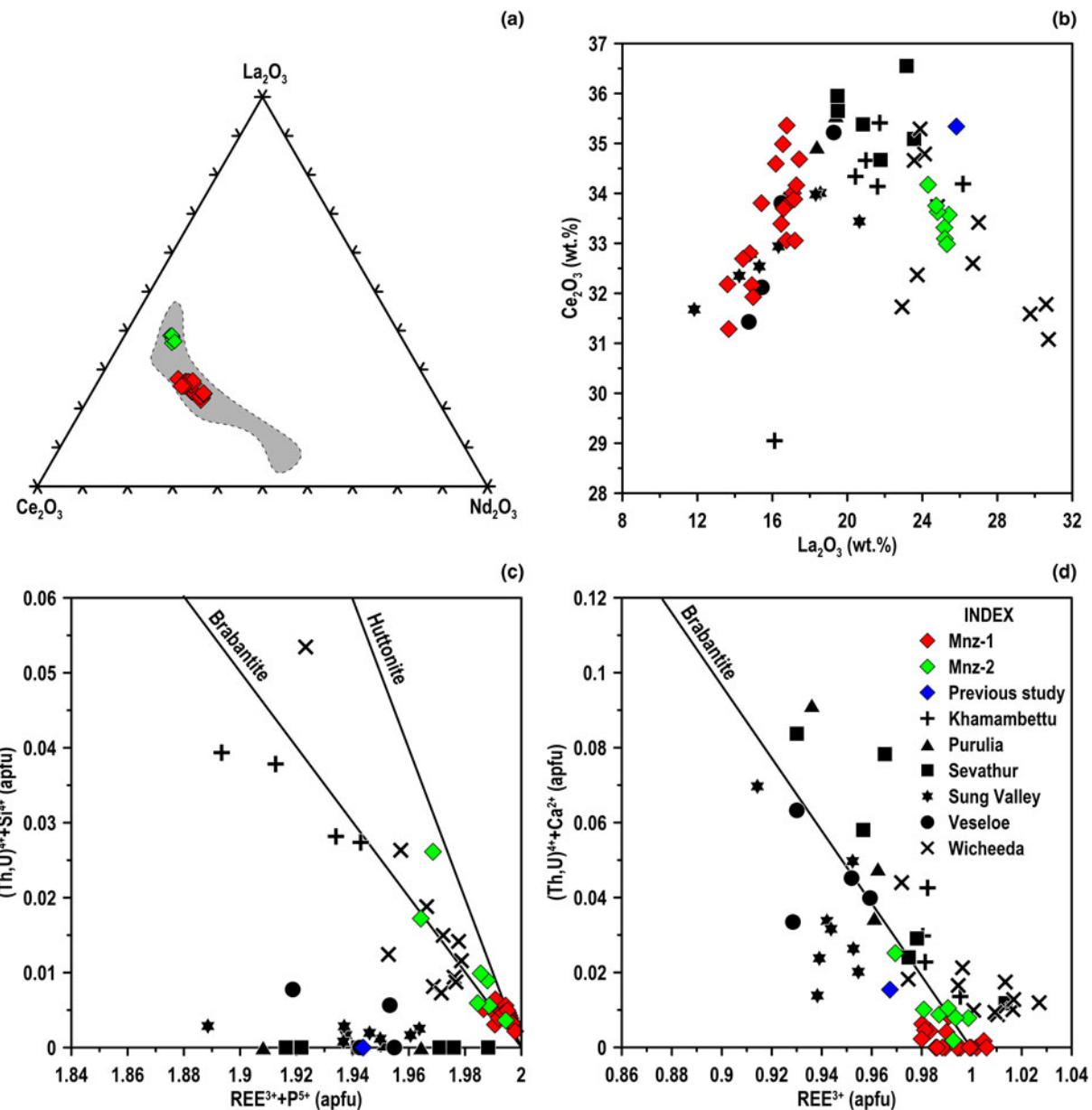


Figure 6. Compositional variation of monazite (Mnz-1 and Mnz-2) from Newania carbonatites: (a) Nd₂O₃-La₂O₃-Ce₂O₃ ternary plot (wt.-%); (b) Ce₂O₃ vs. La₂O₃ (wt.-%); (c) (Th+U)⁴⁺ + Si⁴⁺ vs. ΣREE³⁺ + P⁵⁺ (apfu); (d) (Th+U)⁴⁺ + Ca²⁺ vs. ΣREE³⁺ (apfu). Compositional fields of carbonatite-hosted monazites in Fig. 6a are shown in grey colour and are from Chen *et al.* (2017). The data points of worldwide carbonatite monazites in Fig. 6b-d are from Doroshkevich *et al.* (2007), Burtseva *et al.* (2013), Basu and Bhattacharya (2014), Sadiq *et al.* (2014), Dalsin *et al.* (2015), Trofanenko *et al.* (2016), Rampilova *et al.* (2021); previously published Newania monazite composition are from Sorokhtina *et al.* (2022).

et al. (2022). The Newania pyrochlores are enriched in niobium with Nb>Ti>>Ta, and hence, belong to the pyrochlore-group (Fig. 10a) and are Sr-bearing U-rich kenocalciopyrochlore and Sr-, Ca-bearing U-rich kenopyrochlore. They are characterised by 26.0–28.5 wt.% Nb₂O₅, 12.9–16.0 wt.% Ta₂O₅ and 5.3–6.8 wt.% TiO₂. A-site cations are dominated by Ca (3.9–4.6 wt.% CaO) and U (17.1–19.6 wt.% UO₂). Strontium and Ba contents range up to 4.7 wt.% and 0.9 wt.%, respectively. The contents of Na and REE are <0.5 wt.%.

Pyrochlore in the dolomite carbonatite fall within the hydrothermal to supergene field on a ternary Na – A-site-vacancy – Ca plot and partially overlap with previously published Newania pyrochlore compositions (Fig. 10b; Viladkar and Ghose, 2002; Viladkar *et al.*, 2017). Overall, the Newania pyrochlore compositions are in good

agreement with the carbonatite pyrochlore compositions, worldwide (Fig. 10c). Similar pyrochlore compositions with significant A-site vacancy, Sr, Ba and U are described from carbonatites at Angola (Bambi *et al.*, 2012), Lesnaya Varaka, Kola Peninsula, Russia (Chakhmouradian and Mitchell, 1998), Good Hope, Canada (Mitchell *et al.*, 2020), Catalão I and II, Brazil (Guarino *et al.*, 2017) and Sevathur, Tamil Nadu, India (Viladkar and Bismayer, 2014; Dey *et al.*, 2021; Fig. 10d). Newania pyrochlores analysed in this work and previous studies, together with those from Sevathur and Lesnaya Varaka show an evolutionary trend towards increased Sr and Ba. This is in contrast with the magmatic pyrochlores from Aley (Chakhmouradian *et al.*, 2015), Angolan (Bambi *et al.*, 2012), Catalão I and II (Guarino *et al.*, 2017) and Fir (Chudy, 2014) carbonatites which trend towards F (Fig. 10d).

Table 4. Compositions of amphiboles in dolomite carbonatite, calculated using the amphibole classification spreadsheet of Locock (2014).

| Oxide (wt.%) | LLD (wt.%) | Amp-1 | | | | | | | | Amp-2 | | |
|--------------------------------|------------|-------|-------|-------|-------|-------|-------|-------|-------|-------|-------|-------|
| | | 1 | 2 | 3 | 4 | 5 | 6 | 7 | 8 | 9 | 10 | 11 |
| SiO ₂ | 0.04 | 55.42 | 56.00 | 55.68 | 55.62 | 56.00 | 55.58 | 55.53 | 55.55 | 53.29 | 53.56 | 53.38 |
| TiO ₂ | 0.06 | 0.07 | bdl | bdl | 0.08 | 0.09 | bdl | 0.10 | 0.11 | bdl | bdl | bdl |
| Al ₂ O ₃ | 0.02 | 0.37 | 0.34 | 0.35 | 0.39 | 0.35 | 0.36 | 0.38 | 0.37 | 0.14 | 0.07 | 0.06 |
| FeO | 0.10 | 3.81 | 6.45 | 4.38 | 5.45 | 5.30 | 4.72 | 4.05 | 4.26 | 24.95 | 23.65 | 24.10 |
| Fe ₂ O ₃ | | 9.92 | 6.50 | 9.20 | 7.72 | 7.85 | 8.36 | 9.54 | 9.21 | 1.61 | 3.07 | 2.44 |
| MnO | 0.08 | 0.21 | 0.15 | 0.13 | 0.19 | 0.17 | 0.13 | 0.21 | 0.17 | 0.54 | 0.61 | 0.62 |
| MgO | 0.02 | 16.50 | 15.82 | 16.53 | 16.27 | 16.31 | 16.57 | 16.46 | 16.52 | 14.53 | 14.60 | 14.50 |
| CaO | 0.03 | 4.95 | 4.11 | 5.05 | 5.12 | 5.11 | 4.80 | 4.76 | 5.08 | 0.45 | 0.53 | 0.43 |
| Na ₂ O | 0.05 | 5.31 | 6.30 | 5.40 | 5.39 | 5.29 | 5.73 | 5.57 | 5.26 | 0.82 | 1.11 | 1.02 |
| K ₂ O | 0.05 | 0.58 | 0.60 | 0.53 | 0.65 | 0.60 | 0.64 | 0.53 | 0.63 | bdl | 0.06 | bdl |
| F | 0.12 | n.a. | 0.49 | 0.50 | 0.44 |
| H ₂ O ⁺ | | 2.11 | 2.09 | 2.11 | 2.10 | 2.11 | 2.10 | 2.11 | 2.11 | 1.76 | 1.78 | 1.79 |
| Total | | 99.23 | 98.34 | 99.35 | 98.97 | 99.17 | 98.99 | 99.22 | 99.26 | 98.37 | 99.34 | 98.59 |

Structural formula calculated on the basis of 23 atoms of oxygen

| | Ferri-winchite | | | | | | | | Cummingtonite | | | |
|------------------|----------------|--------|--------|------------------|--------|--------|--------|--------|---------------|--------|-------------|--|
| | Si | Al | Ti | Fe ³⁺ | C-site | B-site | A-site | W-site | OH | F | Sum T,C,B,A | |
| Si | 7.890 | 8.054 | 7.918 | 7.953 | 7.976 | 7.936 | 7.904 | 7.907 | 8.017 | 7.976 | 8.005 | |
| Al | 0.061 | - | 0.058 | 0.047 | 0.024 | 0.060 | 0.063 | 0.062 | - | 0.012 | - | |
| Ti | 0.007 | - | - | - | - | - | 0.010 | 0.011 | - | - | - | |
| Fe ³⁺ | 0.041 | - | 0.024 | - | - | 0.005 | 0.022 | 0.020 | - | 0.012 | - | |
| C-site | | | | | | | | | | | | |
| Ti | - | - | - | 0.009 | 0.010 | - | - | - | - | - | - | |
| Al | - | 0.057 | - | 0.017 | 0.035 | - | - | - | 0.024 | - | 0.011 | |
| Fe ³⁺ | 1.021 | 0.703 | 0.960 | 0.830 | 0.841 | 0.894 | 1.000 | 0.967 | 0.182 | 0.332 | 0.275 | |
| Mn ²⁺ | 0.025 | 0.018 | 0.015 | 0.023 | 0.021 | 0.016 | 0.025 | 0.021 | - | - | - | |
| Fe ²⁺ | 0.453 | 0.775 | 0.521 | 0.652 | 0.631 | 0.564 | 0.482 | 0.507 | 1.535 | 1.427 | 1.473 | |
| Mg | 3.501 | 3.392 | 3.504 | 3.468 | 3.463 | 3.527 | 3.494 | 3.505 | 3.258 | 3.241 | 3.241 | |
| B-site | | | | | | | | | | | | |
| Mn ²⁺ | - | - | - | - | - | - | - | - | 0.068 | 0.077 | 0.078 | |
| Fe ²⁺ | - | - | - | - | - | - | - | - | 1.604 | 1.519 | 1.550 | |
| Ca | 0.756 | 0.633 | 0.770 | 0.784 | 0.780 | 0.733 | 0.726 | 0.774 | 0.072 | 0.085 | 0.069 | |
| Na | 1.244 | 1.367 | 1.230 | 1.216 | 1.220 | 1.267 | 1.274 | 1.226 | 0.239 | 0.319 | 0.297 | |
| A-site | | | | | | | | | | | | |
| Na | 0.220 | 0.389 | 0.257 | 0.280 | 0.241 | 0.320 | 0.264 | 0.226 | - | - | - | |
| K | 0.106 | 0.109 | 0.095 | 0.118 | 0.108 | 0.117 | 0.096 | 0.114 | - | 0.011 | - | |
| O (non-W) | 22.000 | 22.000 | 22.000 | 22.000 | 22.000 | 22.000 | 22.000 | 22.000 | 22.000 | 22.000 | 22.000 | |
| W-site | | | | | | | | | | | | |
| OH | 2.000 | 2.000 | 2.000 | 2.000 | 2.000 | 2.000 | 2.000 | 2.000 | 1.769 | 1.763 | 1.790 | |
| F | - | - | - | - | - | - | - | - | 0.231 | 0.237 | 0.210 | |
| Sum T,C,B,A | 15.325 | 15.497 | 15.352 | 15.397 | 15.350 | 15.439 | 15.360 | 15.340 | 14.999 | 15.011 | 14.999 | |

Fe₂O₃ and FeO calculated on stoichiometric basis; n.a. – not analysed; LLD – lower limit of detection; bdl – below detection limit.

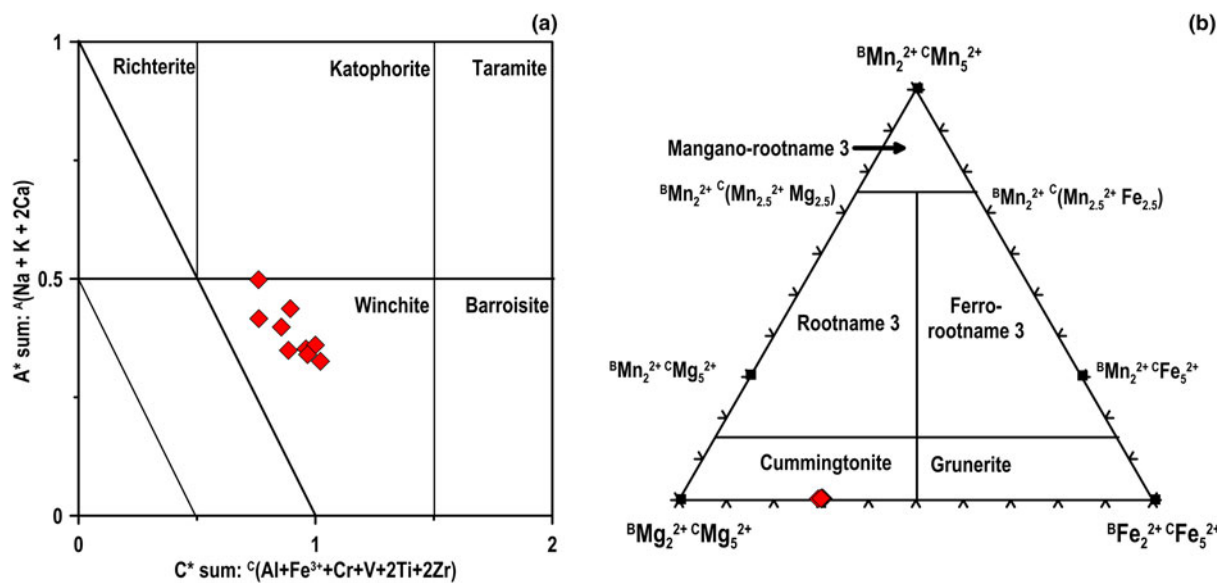


Figure 7. (a,b) Classification diagram for amphiboles in the Newania carbonatites (after Hawthorne et al., 2012).

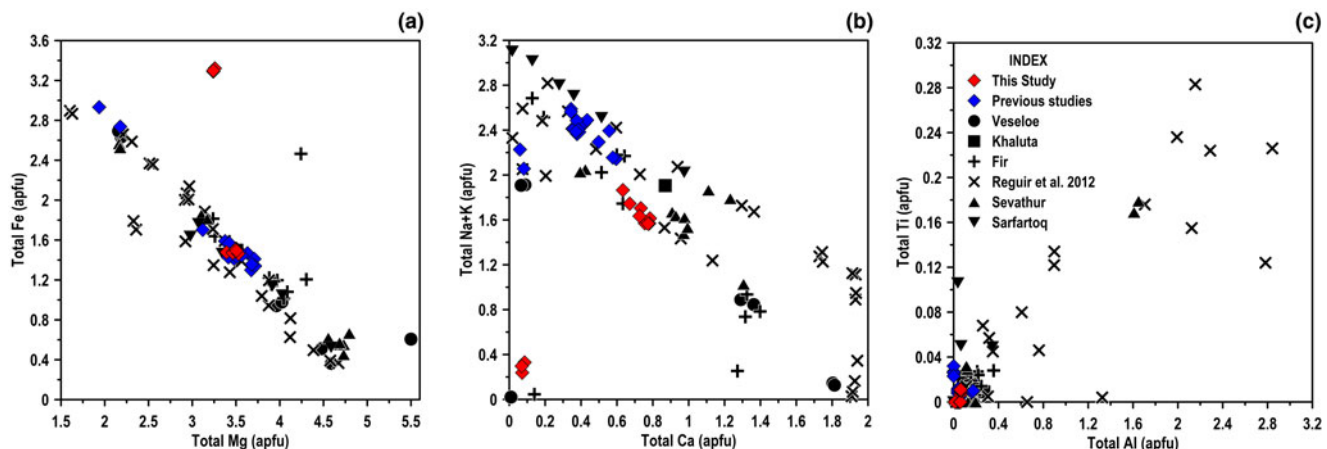


Figure 8. Compositional variation of amphiboles in dolomite carbonatite: (a) Total Fe vs. Total Mg (apfu); (b) Total Na + K vs. Total Ca (apfu); (c) Total Ti vs. Total Al (apfu). Data for worldwide carbonatitic amphiboles are taken from Secher and Larsen (1980), Viladkar and Subramanian (1995), Doroshkevich *et al.* (2007, 2010b), Reguir *et al.* (2012), Chudy (2014), Rampilova *et al.* (2021); previously published data for Newania amphiboles are taken from Viladkar and Wimmenauer (1986); Doroshkevich *et al.* (2010a) and Ray *et al.* (2013).

Discussion

Carbonatites are readily susceptible to textural and chemical re-equilibration during subsolidus, deformational and late-stage hydrothermal conditions (e.g. Chudy, 2014; Chakhmouradian *et al.*, 2016; Mitchell and Smith, 2017). The Newania carbonatite complex presents a similar example where primary textures and mineral compositions are modified and new minerals are crystallised due to post-magmatic processes.

Textural modification

Ferroan dolomite is the principal constituent of the dolomite carbonatite at Newania and illustrates variable degrees of textural re-equilibration. Variation of textures from fractured, euhedral crystals to serrated grain boundaries and thick twinning lamellae to grain boundary bulging, creep and re-crystallisation of very fine carbonates at crystal boundaries attest to the inhomogeneous deformational history of the complex. The conditions of

Table 5. Compositions of columbite-(Fe) in dolomite carbonatite.

| Oxide (wt.%) | LLD (wt.%) | Clb-1 | | | | | | | | | Clb-2 | | | | | |
|---|------------|--------|-------|-------|-------|-------|-------|-------|-------|-------|-------|-------|-------|-------|-------|-------|
| | | 1 | 2 | 3 | 4 | 5 | 6 | 7 | 8 | 9 | 10 | 11 | 12 | 13 | 14 | 15 |
| Nb ₂ O ₅ | 0.08 | 77.30 | 75.86 | 77.08 | 75.65 | 74.47 | 67.94 | 72.07 | 74.19 | 72.94 | 68.39 | 73.70 | 70.37 | 72.04 | 71.73 | 73.86 |
| Ta ₂ O ₅ | 0.37 | 1.67 | 2.06 | 1.59 | 1.69 | 2.91 | 2.73 | 2.82 | 3.38 | 3.38 | 10.04 | 4.50 | 8.04 | 6.12 | 6.30 | 4.52 |
| TiO ₂ | 0.09 | 1.02 | 1.56 | 1.27 | 1.42 | 1.53 | 4.12 | 2.01 | 1.54 | 1.92 | 0.49 | 0.32 | 0.38 | 0.31 | 0.35 | 0.78 |
| UO ₂ | 0.17 | bdl | bdl | bdl | bdl | bdl | 1.87 | 1.00 | bdl |
| Pr ₂ O ₃ | 0.28 | bdl | bdl | bdl | bdl | bdl | bdl | 0.32 | bdl | bdl | bdl | 0.32 | bdl | 0.35 | 0.34 | bdl |
| Y ₂ O ₃ | 0.05 | 0.29 | 0.26 | 0.28 | 0.24 | 0.24 | 0.12 | 0.17 | 0.24 | 0.24 | 0.21 | 0.25 | 0.24 | 0.26 | 0.24 | 0.24 |
| FeO* | 0.12 | 18.67 | 18.56 | 18.68 | 18.58 | 18.31 | 17.71 | 18.64 | 18.22 | 18.10 | 18.36 | 18.86 | 19.14 | 18.95 | 18.69 | 18.74 |
| CaO | 0.07 | bdl | 0.08 | bdl | bdl | bdl | 0.26 | bdl | 0.15 | 0.27 | 0.17 | 0.18 | 0.08 | 0.22 | 0.17 | bdl |
| SrO | 0.13 | bdl | bdl | bdl | bdl | bdl | 0.22 | bdl |
| BaO | 0.11 | bdl | bdl | bdl | bdl | bdl | 0.14 | bdl |
| MgO | 0.03 | 1.13 | 0.74 | 1.08 | 0.94 | 0.79 | 0.24 | 0.33 | 1.05 | 0.88 | 0.99 | 0.78 | 0.70 | 0.75 | 0.85 | 0.90 |
| PbO | 0.16 | 0.23 | 0.27 | bdl | 0.17 | 0.26 | 0.49 | 0.38 | 0.18 | 0.17 | 0.17 | 0.25 | 0.25 | 0.28 | 0.21 | 0.20 |
| K ₂ O | 0.07 | bdl | bdl | bdl | bdl | bdl | 0.06 | bdl |
| Na ₂ O | 0.04 | bdl | bdl | bdl | bdl | bdl | bdl | 0.09 | bdl | bdl | bdl | bdl | bdl | 0.05 | bdl | bdl |
| Total | | 100.32 | 99.39 | 99.97 | 98.68 | 98.50 | 96.33 | 98.11 | 99.13 | 97.78 | 98.90 | 98.84 | 99.61 | 98.76 | 98.98 | 99.74 |
| Structural formula calculated on the basis of 3 cations | | | | | | | | | | | | | | | | |
| Nb | | 1.953 | 1.943 | 1.950 | 1.942 | 1.931 | 1.803 | 1.880 | 1.909 | 1.898 | 1.809 | 1.918 | 1.841 | 1.889 | 1.873 | 1.901 |
| Ta | | 0.025 | 0.032 | 0.024 | 0.026 | 0.045 | 0.044 | 0.044 | 0.052 | 0.053 | 0.160 | 0.070 | 0.127 | 0.097 | 0.099 | 0.070 |
| Ti | | 0.043 | 0.066 | 0.053 | 0.061 | 0.066 | 0.182 | 0.087 | 0.066 | 0.083 | 0.021 | 0.014 | 0.017 | 0.014 | 0.015 | 0.033 |
| U | | - | - | - | - | - | 0.024 | 0.013 | - | - | - | - | - | - | - | - |
| Pr | | - | - | - | - | - | - | - | 0.007 | - | - | - | 0.007 | - | 0.007 | 0.007 |
| Y | | 0.009 | 0.008 | 0.008 | 0.007 | 0.007 | 0.004 | 0.005 | 0.007 | 0.007 | 0.006 | 0.008 | 0.007 | 0.008 | 0.008 | 0.007 |
| Fe ²⁺ | | 0.873 | 0.879 | 0.874 | 0.882 | 0.878 | 0.869 | 0.900 | 0.867 | 0.871 | 0.898 | 0.908 | 0.926 | 0.920 | 0.903 | 0.892 |
| Ca | | - | 0.005 | - | - | - | 0.021 | 0.016 | - | 0.009 | 0.017 | 0.010 | 0.011 | 0.005 | 0.014 | 0.010 |
| Sr | | - | - | - | - | - | 0.012 | 0.007 | - | - | - | - | - | - | - | - |
| Ba | | - | - | - | - | - | 0.008 | 0.003 | - | - | - | - | - | - | - | - |
| Mg | | 0.094 | 0.063 | 0.090 | 0.080 | 0.068 | 0.021 | 0.028 | 0.089 | 0.075 | 0.086 | 0.067 | 0.060 | 0.064 | 0.073 | 0.076 |
| Pb | | 0.003 | 0.004 | - | 0.003 | 0.004 | 0.008 | 0.006 | 0.003 | 0.003 | 0.004 | 0.004 | 0.004 | 0.003 | 0.003 | 0.003 |
| K | | - | - | - | - | - | 0.005 | - | - | - | - | - | - | - | - | - |
| Na | | - | - | - | - | - | - | 0.011 | - | - | - | - | - | - | 0.005 | - |
| Total | | 3.000 | 3.000 | 3.000 | 3.000 | 3.000 | 3.000 | 3.000 | 3.000 | 3.000 | 3.000 | 3.000 | 3.000 | 3.000 | 3.000 | 3.000 |

FeO* is total iron oxide; LLD – lower limit of detection; bdl – below detection limit.

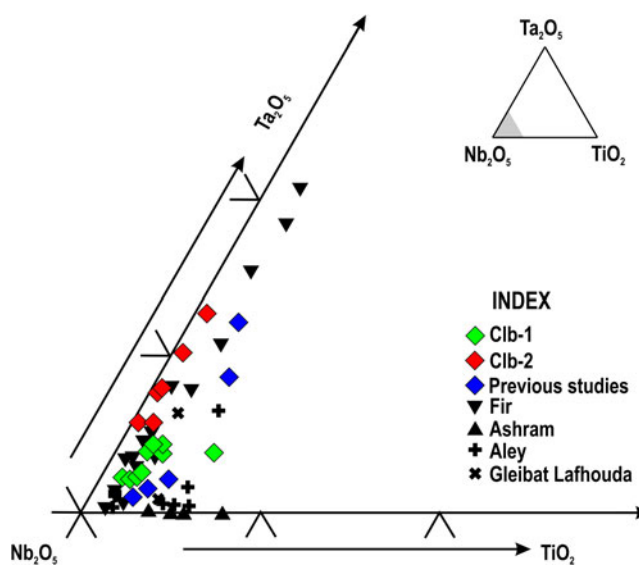


Figure 9. Nb_2O_5 - Ta_2O_5 - TiO_2 ternary diagram showing variation in the compositions of columbite-(Fe) in the Newania carbonatites. Data for columbite in worldwide carbonatites are from Chudy (2014), Chakhmouradian *et al.* (2015), Mitchell and Smith (2017) and Boukrou et al. (2022); previously published data for Newania columbite-(Fe) are from Viladkar *et al.* (2017).

deformation range from brittle to ductile deformation which is accompanied by re-crystallisation at relatively high temperatures (Chakhmouradian *et al.*, 2016). Chudy (2014) has investigated the fabric of Fir carbonatites at megascopic and microscopic levels, and suggested that the observed textures are due to variable degrees of deformation, varying from brittle to plastic-ductile regimes.

Rarely, apatite in dolomite carbonatite displays effects of deformation, such as fractures in Ap-1 and wavy extinction in Ap-2 crystals. However, magmatic textures of apatite are preserved better than those of carbonates which have been modified post-crystallisation. Magmatic textures of apatite include the oval morphology of the crystals and abraded margins at the contact between apatite and ferroan dolomite grains. These are typical of apatite in plutonic carbonatites, produced via erosion/abrasion due to surrounding magma and crystals and/or by unusual growth mechanisms (Chakhmouradian *et al.*, 2017). Such apatite morphologies are significantly different from experimentally produced prismatic apatite with well developed crystal faces (Hammouda *et al.*, 2010; Anenburg *et al.*, 2020). The monomineralic layers of Ap-1 grains are magmatic in origin, formed by the separation of apatite grains from parent magma due to crystal setting (Wyllie and Biggar, 1966).

The textural characteristics of Newania monazite are more similar to hydrothermal monazite than magmatic carbonatite

Table 6. Compositions of pyrochlore in dolomite carbonatite.

| Oxide (wt.%) | LLD (wt.%) | 1 | 2 | 3 | 4 | 5 | 6 | 7 |
|--|------------|-------|-------|-------|-------|-------|-------|-------|
| Na_2O | 0.04 | bdl | 0.14 | 0.10 | bdl | 0.07 | bdl | 0.10 |
| K_2O | 0.07 | bdl | 0.23 | bdl | 0.13 | bdl | 0.09 | bdl |
| CaO | 0.07 | 4.25 | 3.94 | 4.61 | 4.63 | 4.04 | 4.31 | 4.32 |
| SrO | 0.13 | 5.67 | 3.88 | 4.73 | 4.15 | 3.29 | 3.80 | 3.61 |
| BaO | 0.11 | 0.74 | 0.52 | 0.59 | 0.71 | 0.88 | 0.95 | 0.83 |
| PbO | 0.16 | 2.23 | 2.37 | 2.46 | 2.18 | 1.96 | 2.30 | 2.37 |
| Ce_2O_3 | 0.07 | 0.50 | 0.42 | 0.48 | 0.53 | 0.55 | 0.43 | 0.57 |
| UO_2 | 0.17 | 18.36 | 18.86 | 17.05 | 18.28 | 19.04 | 18.34 | 19.65 |
| Al_2O_3 | 0.03 | 0.33 | 0.36 | 0.31 | 0.33 | 0.24 | 0.33 | 0.29 |
| SiO_2 | 0.08 | bdl | bdl | bdl | bdl | 9.91 | 10.26 | 10.02 |
| TiO_2 | 0.09 | 6.74 | 6.20 | 5.32 | 6.41 | 6.84 | 6.27 | 6.83 |
| $\text{Fe}_2\text{O}_3^{\#}$ | - | 2.57 | 2.12 | 2.77 | 2.38 | 1.92 | 2.43 | 2.21 |
| MgO | 0.03 | 0.33 | 0.38 | 0.37 | 0.39 | 0.50 | 0.41 | 0.41 |
| Nb_2O_5 | 0.08 | 27.54 | 26.00 | 28.43 | 26.65 | 27.82 | 27.55 | 28.39 |
| Ta_2O_5 | 0.37 | 13.47 | 13.36 | 13.64 | 13.27 | 14.63 | 15.96 | 12.88 |
| Total | | 80.74 | 78.79 | 80.87 | 80.03 | 91.68 | 93.44 | 92.48 |
| Structural formula calculated on the basis of total B-site cations = 2 | | | | | | | | |
| Na | - | 0.024 | 0.016 | - | 0.008 | - | 0.011 | |
| K | - | 0.026 | - | 0.014 | - | 0.007 | - | |
| Ca | 0.379 | 0.373 | 0.419 | 0.427 | 0.254 | 0.267 | 0.271 | |
| Sr | 0.178 | 0.199 | 0.233 | 0.207 | 0.112 | 0.127 | 0.123 | |
| Ba | 0.024 | 0.018 | 0.020 | 0.024 | 0.020 | 0.021 | 0.019 | |
| Pb | 0.050 | 0.056 | 0.056 | 0.051 | 0.031 | 0.036 | 0.037 | |
| Ce | 0.015 | 0.014 | 0.015 | 0.017 | 0.012 | 0.009 | 0.012 | |
| U | 0.340 | 0.371 | 0.322 | 0.350 | 0.249 | 0.236 | 0.256 | |
| Sum A-site | 0.646 | 0.660 | 0.743 | 0.725 | 0.429 | 0.461 | 0.462 | |
| Al | 0.033 | 0.038 | 0.031 | 0.034 | 0.017 | 0.023 | 0.020 | |
| Si | - | - | - | - | 0.581 | 0.593 | 0.587 | |
| Ti | 0.423 | 0.412 | 0.340 | 0.415 | 0.302 | 0.272 | 0.301 | |
| Fe^{3+} | 0.161 | 0.141 | 0.177 | 0.154 | 0.085 | 0.106 | 0.098 | |
| Mg | 0.041 | 0.050 | 0.047 | 0.050 | 0.044 | 0.036 | 0.036 | |
| Nb | 1.037 | 1.038 | 1.091 | 1.037 | 0.738 | 0.720 | 0.752 | |
| Ta | 0.305 | 0.321 | 0.315 | 0.311 | 0.233 | 0.251 | 0.205 | |
| Sum B-site | 2.000 | 2.000 | 2.000 | 2.000 | 2.000 | 2.000 | 2.000 | |

$\text{Fe}_2\text{O}_3^{\#}$ is total iron, calculated from FeO ; lower limit of detection for FeO is 0.12 wt.%; LLD – lower limit of detection; bdl – below detection limit.

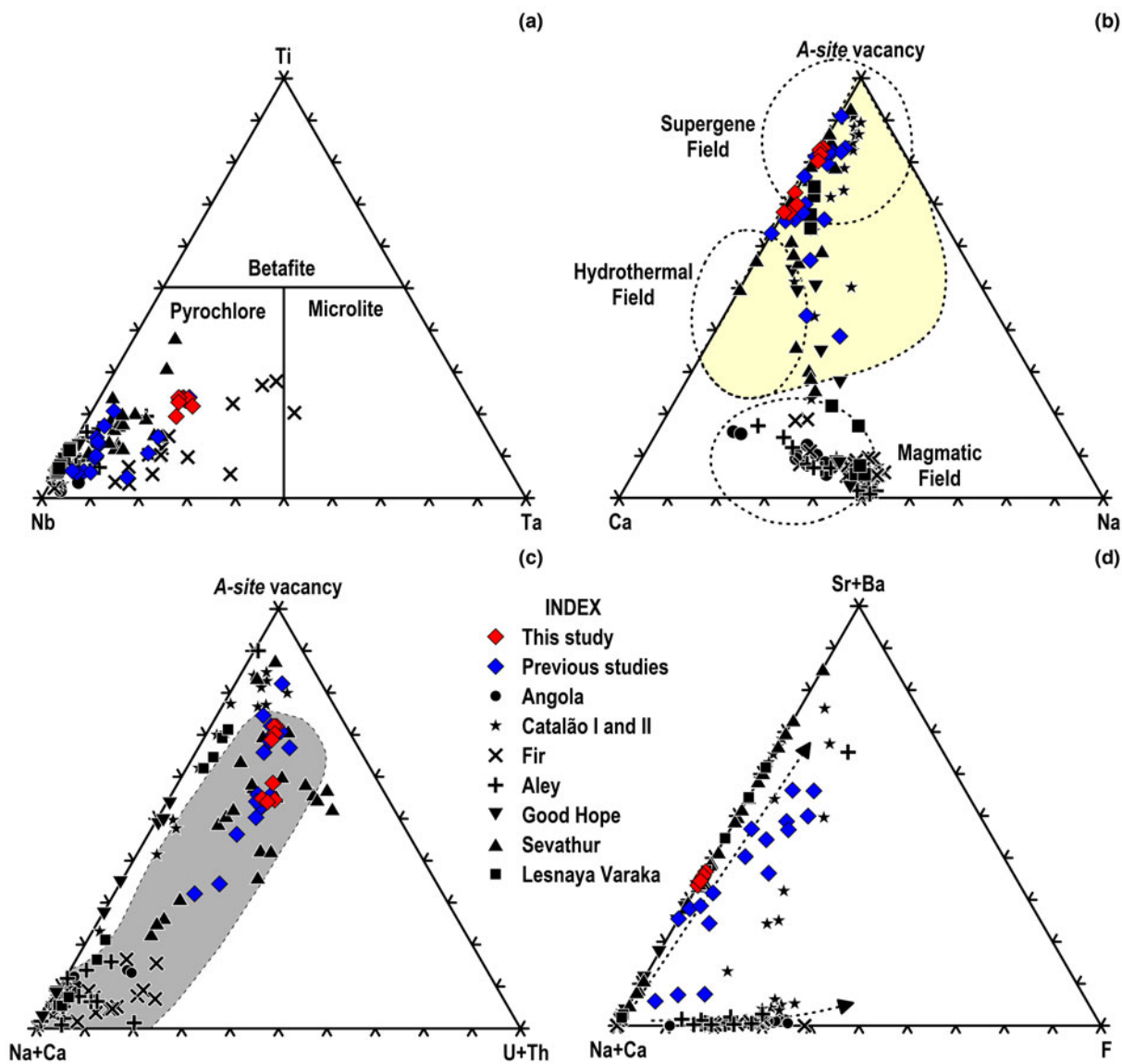


Figure 10. Ternary compositional diagrams for pyrochlores in dolomite carbonatite at Newania: (a) Nb–Ti–Ta (apfu); (b) Ca – A-site-vacancy – Na (apfu); (c) Na+Ca – A-site-vacancy – U+Th (apfu); (d) Na+Ca – Sr+Ba – F (apfu). Fields in (a) are from Atencio *et al.* (2010), dotted-line and yellow fields in (b) are from Zurevinski and Mitchell (2004) and Bhattacharjee *et al.* (2022), respectively and grey field in (c) is taken from Chakhmouradian and Mitchell (2002); pyrochlore compositional data are taken from Chakhmouradian and Mitchell (1998), Bambi *et al.* (2012), Chudy (2014), Viladkar and Bismayer (2014), Chakhmouradian *et al.* (2015) and Mitchell *et al.* (2020); previously published data for Newania pyrochlores are taken from Viladkar and Ghose (2002) and Viladkar *et al.* (2017).

monazites, such as having localised aggregates of more than four grains, high relief and birefringence and weak pleochroism (Schandl and Gorton, 2004; Kim *et al.*, 2005; Xu *et al.*, 2010; Giebel *et al.*, 2017; Slezak and Spandler, 2019). The dissolution of precursor mineral(s) and re-precipitation of new or altered phases result in porosity development. The mechanism of porosity development is discussed in Harlov *et al.* (2002), Putnis (2002) and Harlov (2011, 2015). Porous textures are evident in monazite in Newania carbonatite and indicate a non-magmatic origin. Inhomogeneous intra-intrusion distribution and exclusive occurrence with apatite as anhedral inclusions at grain boundaries of Ap-1, commonly penetrating the grains or as pseudomorphs after the Ap-2 attest to the post-magmatic origin of monazite. The presence of hydrothermal monazite (Mnz-1) with deformed Ap-1 grains indicates the involvement of a fluid phase during or after

the deformation. Experimental studies have shown that monazite can crystallise over a range of temperature and pressure varying from 300 to 900°C and 500 to 1000 MPa, respectively; and, the fluid facilitating monazite crystallisation is characterised by pure H₂O to diluted solutions with CO₂ or KCl and can be REE-rich (Harlov and Förster, 2003; Trofanenko *et al.*, 2016).

The columbite–pyrochlore composite grains exhibit variable proportions and intergrowth patterns but no core–rim structure and fine veinlet network; hence, they are not replacing each other (Chudy, 2014) and are altered during late-to-post magmatic stages. However, the effects of alteration are much more prominent for pyrochlore than columbite-(Fe), as indicated by the porous texture and composition of pyrochlore (discussed below). Unlike carbonates and apatite, columbite-(Fe) and pyrochlore are relatively more resistant to deformation. Baryte is exclusively present

at peripheral regions of composite grains, constituting post-magmatic mineral assemblage with monazite.

Mineralogical evolution

Carbonatitic apatite are characterised by Cl-poor fluorapatite or F-rich hydroxylapatite compositions, containing 0.2–2.7 wt.% SrO, up to 4.5 wt.% REE_2O_3 and 0.8 wt.% Na₂O (Chakhmouradian *et al.*, 2017). Newania apatite fall well within the compositional range of magmatic apatite in carbonatites except for depletion in REE. Secondary apatite in carbonatites can crystallise by solution and reprecipitation of primary fluorapatite (Basu and Bhattacharya, 2014) and show enrichment in heavy REE contents, such as in the case of the Songwe Hill, Tundulu and Kangankunde carbonatite complexes in Malawi (Broom-Fendley *et al.*, 2016, 2017). However, no such compositional features are evident in Newania apatite, indicating negligible effects of deformation on composition.

Amphiboles in the Newania carbonatites are of both magmatic and metamorphic origin. Ferri-winchite, together with previously published amphibole compositions viz. ferri-katophorite, magnesio-arfvedsonite and magnesio-riebeckite (Viladkar and Wimmenauer, 1986; Doroshkevich *et al.*, 2010a; Ray *et al.*, 2013) are magmatic amphiboles and represent the middle-to-late stage of amphibole crystallisation from parent carbonatite-forming melt (Samoylov, 1977; Martin, 2007). The low contents of Al and Ti indicate no assimilation and contamination of parent carbonatite magma by crustal material (Chakhmouradian and Zaitsev, 2002; Chudy, 2014). Cummingtonite is a metamorphic amphibole, rare among igneous rocks and crystallises under regional metamorphic conditions in low-Ca amphibolites (Deer *et al.*, 2013). There is no textural evidence to verify if the early crystallised magmatic amphiboles are later replaced by cummingtonite. Examples of metamorphic amphiboles in carbonatites are not common. Lastochkin *et al.* (2011) and Chudy (2014) have reported metamorphic amphiboles, compositionally equivalent to tremolite–actinolite and anthophyllite. Chudy (2014) postulated the origin of tremolite–actinolite in the presence of ferroan dolomite during metamorphic growth.

The Newania pyrochlores have U–Ta–Ti-rich compositions and significant A- and Y-site vacancies which show that the pyrochlores are magmatic in nature and have undergone alteration

during late-to-post magmatic conditions. The U–Ta–Ti-rich compositions are indicative of early-stage crystallisation from the parent carbonatite magma (Chakhmouradian and Mitchell, 1998) as the contents of U and B-site cations remain constant during alteration (Lumpkin and Ewing, 1995). The development of vacancies at A- and Y-sites is a consequence of secondary alteration indicated by the leaching of cations and anions, cation exchange and hydration (Lumpkin and Ewing, 1995; Chakhmouradian and Mitchell, 1998). Nasraoui and Bilal (2000) have described similar supergene alteration of carbonatitic pyrochlore in the Lueshe carbonatite complex (Democratic Republic of Congo). The source for U, Ta and Nb must be the parental carbonatite-forming magma as no other U-bearing phases are present. Hence, it is unlikely that the U-enrichment in Newania pyrochlores is secondary in nature.

The compositional data for columbite–tantalite-group minerals from carbonatites are available for only a few occurrences (Chudy, 2014; Chakhmouradian *et al.*, 2015; Mitchell and Smith, 2017; Boukirou *et al.*, 2022), and data on co-crystallisation of columbite and pyrochlore in carbonatite is even rarer. Experimental work of Lumpkin and Ewing (1995) shows that pyrochlore can co-exist with columbite-(Fe) under moderate $a_{\text{Fe}^{2+}}$ and $a_{\text{Ca}^{2+}}$ and low-to-moderate a_{Na^+} conditions. Chudy (2014) has postulated that under decreasing a_{Na^+} / $a_{\text{Ca}^{2+}}$ conditions, columbite-(Fe) and pyrochlore can become stable.

Crystallisation sequence

The crystallisation sequence of minerals in Newania carbonatites as interpreted from textural and compositional data is given in Fig. 11. The earliest crystallising phase in dolomite carbonatite is Ap-1 which formed bands/layers in the north-western region of the complex. This was followed by the crystallisation of Amp-1 and columbite–pyrochlore composite grains. Ap-2 and magnesian siderite are co-crystallised. Clb-2, which occurs as individual grains of columbite is formed later than Clb-1. Ferroan dolomite displays an extended crystallising history and crystallised always after the non-carbonate phases. Monazite is a hydrothermal phase which crystallised during the post-magmatic stage of carbonatite evolution. These monazite grains are not deformed whereas the surrounding Ap-1 and ferroan dolomite grains show deformation features, and hence are crystallised later

| Mineral assemblage | Magmatic stage | Post-magmatic stage |
|--------------------|-----------------|------------------------|
| Ferroan dolomite | — | |
| Magnesian siderite | — | |
| Apatite | Ap-1 | Ap-2 |
| Amphibole | Amp-1 | Amp-2 |
| Columbite-(Fe) | Clb-1 | |
| Pyrochlore | Clb-2 | |
| Monazite | Composite-grain | Mnz-1 Mnz-2 |
| Baryte | | Rim on composite-grain |

Figure 11. Schematic diagram showing crystallisation sequence of constituent minerals in dolomite carbonatite at Newania.

than the deformation event. Baryte is a late-stage phase which crystallised as a rim on columbite–pyrochlore composite grains.

Origin of Newania carbonatites

The origin of carbonatites from mantle-derived magmas might be explained by three processes: (1) direct low-degree partial melting of carbonated peridotite at mantle depths exceeding 70 kms (e.g. Wyllie and Huang, 1975; Wallace and Green, 1988); (2) separation of conjugate silicate and carbonate magma from parent carbonated silicate magma by liquid immiscibility (e.g. Kjarsgaard and Peterson, 1991; Mitchell, 2009; Weidendorfer *et al.*, 2017); and (3) generation of carbonatitic residual magma by fractional crystallisation of carbonated silicate magma (e.g. Watkinson and Wyllie, 1971; Mitchell, 2005). The nature of the parental magma of the Newania carbonatites is indicated by the dominance of dolomite carbonatite and the absence of genetically-related silicate rock(s). This observation suggests derivation of a parent magma directly by melting of mantle peridotite.

Experimental studies (Wyllie and Huang, 1975; Wallace and Green, 1988) have shown that primary carbonate-bearing magmas can be generated by low-degree partial melting of carbonate-amphibole-bearing lherzolite, containing 0.3% H₂O and 0.5–2.5% CO₂ at pressures between 2.1 to 3 GPa and temperatures ranging from 930 to 1080°C. Such carbonatite magma has a dolomitic composition, with high contents of Ca, Mg, Na and Fe (decreasing abundance) and minor K and P, which crystallises dolomite (FeO = 4.4 wt.%) and Na–Mg carbonates. The presence of H₂O and CO₂ as volatile species in the experiments represent fairly oxidising conditions in the mantle source. Brey *et al.* (1983) concluded that the carbonatite magma generated from phlogopite-bearing mantle peridotite becomes more magnesian as the carbonate phase changes from dolomite to magnesite at ~3.2 GPa. Falloon and Green (1990) and Jago and Gittins (1991) have demonstrated that F plays an important role in lowering of liquidus temperature of carbonates whereas H₂O has little effect on peridotite solidus, thus indicating low solubility of H₂O in carbonatite magma.

The mineralogy of dolomite carbonatite contains significant modal abundances of F-bearing non-carbonate phases such as apatite and amphibole, indicating presence of F, P, Si and alkalis (Na>K) in the parent magma. These observations are consistent with the experimentally produced carbonatite magma compositions of Wallace and Green (1988). The crystallisation of magmatic magnesian siderite is possible only from a carbonatite magma with high magnesian content. Such magma might be produced from magnesite–phlogopite-bearing mantle peridotite at depths exceeding 3.2 GPa (Brey *et al.*, 1983; Buckley and Woolley, 1990; Woolley and Buckley, 1993). The occurrence of Ap-1 and pyrochlore as early-crystallised phases suggest that the parent magma inherently contains a few percent of phosphate and fluorine (Wyllie and Biggar, 1966; Jago and Gittins, 1993; Mitchell and Kjarsgaard, 2004). On the basis of mineralogical studies and previously published literature for the Newania carbonatites, it is concluded that the parent magma for Newania carbonatites is produced by low-degree partial melting of magnesite–phlogopite-bearing peridotite at pressures reaching up to 3 GPa. The magma generated is dolomitic in composition, possibly more magnesian in composition and contains significant contents of Si, F, P and alkalis (Na and K).

The dolomite carbonatite occurrences at Gleibat Lafhouda (~1.85 Ga; Montero *et al.*, 2016) and Veseloe (~593 Ga;

Doroshkevich *et al.*, 2007) are similar to the Newania carbonatites. Both of these carbonatite occurrences are exclusively dolomite carbonatite-dominated complexes, devoid of genetically-related silicate rock(s) and emplaced in an extensional environment (Doroshkevich *et al.*, 2007; Boukirou *et al.*, 2022). Doroshkevich *et al.* (2007) have postulated that the calcite-bearing dolomite carbonatite at Veseloe has crystallised from a rapidly transported dolomitic magma that originated within the mantle. Boukirou *et al.* (2022) have suggested a similar origin for the Gleibat Lafhouda dolomite carbonatites, stating crystallisation from an Mg-rich magma, originated by very low-degree partial melting of mantle containing garnet and phlogopite. Furthermore, the emplacement coincides with the plume-initiated breakup of the Columbia supercontinent (ca. 1.85 Ga). Laiwu-Zibo carbonatites (China) are another example of such mantle-derived carbonatites. These consist of a complete carbonatite series of calcio-, magnesio- and ferrocarbonatites which are suggested to be generated directly from partial melting of Mesozoic enriched lithosphere (Ying *et al.*, 2004).

Conclusions

The Newania carbonatite complex is a plutonic carbonatite occurrence consisting principally of ferroan dolomite carbonatite with lesser ferrocarbonatite. The complex has undergone post-emplacement deformation which has affected the original textures and compositions of constituent minerals and resulted in the crystallisation of new minerals. Ferroan dolomite has undergone a maximum degree of deformation, ranging from brittle-to-ductile deformation regimes and subsequent re-crystallisation. Two types of apatite, Ap-1 and Ap-2 crystallised during the early- and late-stages of carbonatite evolution, respectively. Two new compositions of amphiboles viz. ferri-winchite and cummingtonite are found where the former has a magmatic origin and the latter probably crystallised during deformation. Pyrochlore is a magmatic phase, crystallised during early stages of evolution, which has undergone supergene alteration during late- to post-magmatic stages. However, the U-Ta-Ti-rich signature of magmatic origin remained unchanged during alteration. Monazite and baryte constitute a post-magmatic mineral assemblage. The parent melt for Newania carbonatites is considered to be a silica-bearing magnesian carbonate magma derived from low degree partial melting of magnesite–phlogopite-bearing peridotite at pressures equivalent to 3 GPa.

Acknowledgements. AS is thankful to the Council of Scientific and Industrial Research, Government of India for providing fellowship for doctoral work. The authors express their gratitude to Prof. Suresh C. Patel of IIT, Bombay for generating EPMA data. AS and DSS acknowledge the Director, CSIR-NGRI, Hyderabad for providing permission to use analytical facilities at NGRI. AS thanks Parminder Kaur, Sanchit Garg, Jaspreet Saini and Praveen Tantkar for help and guidance during fieldwork. Two anonymous Journal reviewers, Associate Editor Leone Melluso and Production Editor Helen Kerbey are thanked for providing comments and suggestions. Principal Editor Stuart Mills is thanked for editorial handling.

Supplementary material. The supplementary material for this article can be found at <https://doi.org/10.1180/mgm.2023.61>.

Competing interests. The authors declare none.

References

- Ahmad I., Mondal M.E.A., Rahaman M.S., Bhutani R. and Satyanarayanan M. (2020) Archean granitoids of the Aravalli Craton, northwest India. *Geological Society, London, Special Publications*, **489**, 215–234.

- Annenburg M., Mavrogenes J.A., Frigo C. and Wall F. (2020) Rare earth element mobility in and around carbonatites controlled by sodium, potassium, and silica. *Science Advances*, **6**, eabb6570. doi: 10.1126/sciadv.abb6570
- Atencio D., Andrade M.B., Christy A.G., Gieré R. and Kartashov P.M. (2010) The pyrochlore supergroup of minerals: nomenclature. *The Canadian Mineralogist*, **48**, 673–698.
- Bambi A.C.J.M., Costanzo A., Gonçalves A.O. and Melgarejo J.C. (2012) Tracing the chemical evolution of primary pyrochlore from plutonic to volcanic carbonatites: the role of fluorine. *Mineralogical Magazine*, **76**, 377–392.
- Basu S.K. and Bhattacharya T. (2014) Petrography and mineral chemistry of alkaline-carbonatite complex in Singhbhum crustal province, Purulia region, eastern India. *Journal of Geological Society of India*, **83**, 54–70.
- Bell K. and Simonetti A. (2010) Source of parental melts to carbonatites—critical isotopic constraints. *Mineralogy and Petrology*, **98**, 77–89.
- Bhattacharjee S., Dey M., Chakrabarty A., Mitchell R.H. and Ren M. (2022) Zero-valent-dominant pyrochlorites: Endmember formula calculation and petrogenetic significance. *The Canadian Mineralogist*, **60**, 469–484.
- Boukirou W., Bouabdellah M., Chakhmouradian A. R., Mouttaqi A., Reguir E.P., Hauff F., Cuney M., J'ebrik M., Yans J. and Hoernle K. (2022) Petrogenesis of the late Paleoproterozoic Gleibat Lafhouda dolomite carbonatite (West African Craton Margin, Moroccan Sahara) and its relevance to the onset of fragmentation of the Columbia supercontinent. *Chemical Geology*, **594**, 120764. doi:10.1016/j.chemgeo.2022.120764
- Brey G., Brice W.R., Ellis D.J., Green D.H., Harris K.L. and Ryabchikov I.D. (1983) Pyroxene-carbonate reactions in the upper mantle. *Earth and Planetary Science Letters*, **62**, 63–74.
- Broom-Fendley S., Styles M.T., Appleton J.D., Gunn G. and Wall F. (2016) Evidence for dissolution-reprecipitation of apatite and preferential LREE mobility in carbonatite-derived late-stage hydrothermal processes. *American Mineralogist*, **101**, 596–611.
- Broom-Fendley S., Brady A.E., Wall F., Gunn G. and Dawes W. (2017) REE minerals at the Songwe Hill carbonatite, Malawi: HREE-enrichment in late-stage apatite. *Ore Geology Reviews*, **81**, 23–41.
- Buckley H.A. and Woolley A.R. (1990) Carbonates of the magnesite–siderite series from four carbonatite complexes. *Mineralogical Magazine*, **54**, 413–418.
- Buick I.S., Allen C., Pandit M.K., Rubatto D. and Hermann J. (2006) The Proterozoic magmatic and metamorphic history of the Banded Gneiss Complex, central Rajasthan, India: LA-ICP-MS U–Pb zircon constraints. *Precambrian Research*, **151**, 119–142.
- Burtseva M.V., Ripp G.S., Doroshkevich A.G., Viladkar S.G. and Varadan R. (2013) Features of mineral and chemical composition of the Khamambettu Carbonatites, Tamil Nadu. *Journal of Geological Society of India*, **81**, 655–664.
- Chakhmouradian A.R. and Mitchell R.H. (1998) Lueshite, pyrochlore and monazite-(Ce) from apatite-dolomite carbonatite, Lesnaya Varaka complex, Kola Peninsula, Russia. *Mineralogical Magazine*, **62**, 769–782.
- Chakhmouradian A.R. and Mitchell R.H. (2002) New data on pyrochlore-and perovskite-group minerals from the Lovozero alkaline complex, Russia. *European Journal of Mineralogy*, **14**, 821–836.
- Chakhmouradian A.R. and Zaitsev A.N. (2002) Calcite–amphibole–clinopyroxene rock from the Afrikanda complex, Kola Peninsula, Russia: mineralogy and a possible link to carbonatites. III. Silicate minerals. *The Canadian Mineralogist*, **40**, 1347–1374.
- Chakhmouradian A.R. and Zaitsev A.N. (2012) Rare earth mineralization in igneous rocks; sources and processes. *Elements*, **8**, 347–353.
- Chakhmouradian A.R., Böhm C.O., Demény A., Reguir E.P., Hegner E., Creaser R.A., Halden N.M. and Yang P. (2009) “Kimberlite” from Wekusko Lake, Manitoba: actually a diamond-indicator-bearing dolomite carbonatite. *Lithos*, **112**, 347–357.
- Chakhmouradian A.R., Reguir E.P., Kressall R.D., Crozier J., Pisiak L.K., Sidhu R. and Yang P. (2015) Carbonatite-hosted niobium deposit at Aley, northern British Columbia (Canada): Mineralogy, geochemistry and petrogenesis. *Ore Geology Reviews*, **64**, 642–666.
- Chakhmouradian A.R., Reguir E.P. and Zaitsev A.N. (2016) Calcite and dolomite in intrusive carbonatites. I. Textural variations. *Mineralogy and Petrology*, **110**, 333–360.
- Chakhmouradian A.R., Reguir E.P., Zaitsev A.N., Couëslan C., Xu C., Kynicky J., Hamid Mumin A. and Yang P. (2017) Apatite in carbonatitic rocks: Compositional variation, zoning, element partitioning and petrogenetic significance. *Lithos*, **274**, 188–213.
- Chen W., Honghui H., Bai T. and Jiang S. (2017) Geochemistry of monazite within carbonatite related REE deposits. *Resources*, **6**, 51, doi:10.3390/resources6040051
- Chudy T.C. (2014) *The petrogenesis of the Ta-bearing Fir carbonatite system, east-central British Columbia, Canada*. PhD Thesis, University of British Columbia, Canada.
- Chukanov N., Pasero M., Aksenov S., Britvin S., Zubkova N., Yike L. and Witzke T. (2023) Columbite supergroup of minerals: Nomenclature and classification. *Mineralogical Magazine*, **87**, 18–33, doi:10.1180/mgm.2022.105
- Dalsin M.L., Groat L.A., Creighton S. and Evans R.J. (2015) The mineralogy and geochemistry of the Wicheeda carbonatite complex, British Columbia, Canada. *Ore Geology Reviews*, **64**, 523–542.
- Dar K.K. (1964) Some geological data on Atomic Energy minerals in India. *Geological Society of India*, **5**, 112–120.
- Deans T. and Powell J.L. (1968) Trace elements and strontium isotopes in carbonatites, fluorites and limestones from India and Pakistan. *Nature*, **218**, 750–752.
- Deer W.A., Howie R.A. and Zussman J. (2013) *An Introduction to the Rock-Forming Minerals*. The Mineralogical Society, London, 549 pp.
- Dey M., Bhattacharjee S., Chakrabarty A., Mitchell R.H., Pal S., Pal S. and Sen A.K. (2021) Compositional variation and genesis of pyrochlore, belkovite and baotite from the Sevattur carbonatite complex, India. *Mineralogical Magazine*, **85**, 588–606.
- Dharma Rao C.V., Santosh M., Purohit R., Wang J., Jiang X. and Kusky T. (2011) LA-ICP-MS U–Pb zircon age constraints on the Paleoproterozoic and Neoarchean history of the Sandmata Complex in Rajasthan within the NW Indian Plate. *Journal of Asian Earth Sciences*, **42**, 286–305.
- Doroshkevich A.G., Wall F. and Ripp G.S. (2007) Calcite-bearing dolomite carbonatite dykes from Veseloe, North Transbaikalia, Russia and possible Cr-rich mantle xenoliths. *Mineralogy and Petrology*, **90**, 19–49.
- Doroshkevich A.G., Ripp G. and Viladkar S. (2010a) Newania carbonatites, Western India: example of mantle derived magnesium carbonatites. *Mineralogy and Petrology*, **98**, 283–295.
- Doroshkevich A.G., Ripp G.S. and Moore K.R. (2010b) Genesis of the Khaluta alkaline-basic Ba–Sr carbonatite complex (west Transbaikala, Russia). *Mineralogy and Petrology*, **98**, 245–268.
- Falloon T.J. and Green D.H. (1990) Solidus of carbonated fertile peridotite under fluid-saturated conditions. *Geology*, **18**, 195–199.
- Fareeduddin and Banerjee D.M. (2020) Aravalli craton and its mobile belts: An update. *Episodes Journal of International Geoscience*, **43**, 88–108.
- Fareeduddin and Krone A. (1998) Single zircon age constraints on the evolution of the Rajasthan granulites. Pp 547–556 in: *The Indian Precambrian Jodhpur, India*, (B. S. Paliwal, editor) Scientific Publications.
- Fosu B.R., Ghosh P., Chew D.M. and Viladkar S.G. (2019) Composition and U—Pb ages of apatite in the Amba Dongar carbonatite–alkaline complex, India. *Geological Journal*, **54**, 3438–3454.
- Giebel R.J., Gauert C.D., Marks M.A., Costin G. and Markl G. (2017) Multi-stage formation of REE minerals in the Palabora Carbonatite Complex, South Africa. *American Mineralogist*, **102**, 1218–1233.
- Gruau G., Petibon C., Viladkar S., Fourcade S., Bernard-Griffiths J. and Mace J. (1995) Extreme isotopic signatures in carbonatites from Newania, Rajasthan. *Terra Nova*, **7**(Suppl. 1), 336.
- GSI (2011) *Geology and Mineral Resources of Rajasthan*. Geological Survey of India, Miscellaneous Publications No. 30, Part 12, 3rd revised edition, 130 pp.
- Guarino V., Wu F.Y., Melluso L., de Barros Gomes C., Tassinari C.C.G., Ruberti E. and Brilli M. (2017) U–Pb ages, geochemistry, C–O–Nd–Sr–Hf isotopes and petrogenesis of the Catalão II carbonatitic complex (Alto Paranaíba Igneous Province, Brazil): implications for regional-scale heterogeneities in the Brazilian carbonatite associations. *International Journal of Earth Sciences*, **106**, 1963–1989.
- Gupta B.C. (1934) *The Geology of Central Mewar*. Memoirs of the Geological Society of India, 107–168 pp.
- Hammouda T., Chantel J. and Devidal J.L. (2010) Apatite solubility in carbonatitic liquids and trace element partitioning between apatite and carbonatite at high pressure. *Geochimica et Cosmochimica Acta*, **74**, 7220–7235.

- Harlov D.E. (2011) Formation of monazite and xenotime inclusions in fluorapatite megacrysts, Gloserhei Granite Pegmatite, Froland, Bamble Sector, southern Norway. *Mineralogy and Petrology*, **102**, 77–86.
- Harlov D.E. (2015) Apatite: A fingerprint for metasomatic processes. *Elements*, **11**, 171–176.
- Harlov D.E. and Förster H.J. (2003) Fluid-induced nucleation of (Y+REE)-phosphate minerals within apatite: Nature and experiment. Part II. Fluorapatite. *American Mineralogist*, **88**, 1209–1229.
- Harlov D.E., Andersson U.B., Förster H.J., Nyström J.O., Dulski P. and Broman C. (2002) Apatite-monazite relations in the Kiirunavaara magnetite-apatite ore, northern Sweden. *Chemical Geology*, **191**, 47–72.
- Hawthorne F.C., Oberti R., Harlow G.E., Maresch W.V., Martin R.F., Schumacher J.C., and Welch M.D. (2012) Nomenclature of the amphibole supergroup. *American Mineralogist*, **97**, 2031–2048.
- Heron A.M. (1953) The geology of central Rajputana. *Memoirs of the Geological Society of India*, **79**, 339.
- Jago B.C. and Gittins J. (1991) The role of fluorine in carbonatite magma evolution. *Nature*, **349**, 56–58.
- Jago B.C. and Gittins J. (1993) Pyrochlore crystallization in carbonatites: the role of fluorine. *South African Journal of Geology*, **96**, 149–160.
- Kim S.J., Lee H.K., Yin J. and Park J.K. (2005) Chemistry and origin of monazites from carbonatite dikes in the Hongcheon-Jaeun district, Korea. *Journal of Asian Earth Sciences*, **25**, 57–67.
- Kjarsgaard B. and Peterson T. (1991) Nephelinite-carbonatite liquid immiscibility at Shombole volcano, East Africa: Petrographic and experimental evidence. *Mineralogy and Petrology*, **43**, 293–314.
- Krishnamurthy P. (2019) Carbonatites of India. *Journal of Geological Society of India*, **94**, 117–138.
- Lastochkin E.I., Ripp G.S. and Doroshkevich A.G. (2011) Mineralogy of metamorphosed carbonatite of the Vesely occurrence, Northern Transbaikal region, Russia. *Geology of Ore Deposits*, **53**, 236–247.
- Le Maitre R. (2002) *Igneous Rocks: A Classification and Glossary of Terms: Recommendations of the International Union of Geological Sciences Subcommission on the Systematics of Igneous Rocks* (2nd ed.). Cambridge University Press, Cambridge, UK.
- Locock A.J. (2014) An Excel spreadsheet to classify chemical analyses of amphiboles following the IMA 2012 recommendations. *Computers & Geosciences*, **62**, 1–11.
- Lumpkin G.R. and Ewing R.C. (1995) Geochemical alteration of pyrochlore group minerals: pyrochlore subgroup. *American Mineralogist*, **80**, 732–743.
- Martin R.F. (2007) Amphiboles in the igneous environment. Pp. 323–358 in: *Amphiboles: crystal chemistry, Occurrence and Health Issues* (Hawthorne, F.C., Oberti, R., Della Ventura, G. and Mottana, A. editors). Reviews in Mineralogy and Geochemistry, **67**. Mineralogical Society of America and the Geochemical Society, Chantilly, Virginia, USA.
- Melluso L., Srivastava R.K., Guarino V., Zanetti A. and Sinha A.K. (2010) Mineral compositions and petrogenetic evolution of the ultramafic-alkaline-carbonatitic complex of Sung Valley, northeastern India. *The Canadian Mineralogist*, **48**, 205–229.
- Mitchell R.H. (2005) Carbonatites and carbonatites and carbonatites. *The Canadian Mineralogist*, **43**, 2049–2068.
- Mitchell R.H. (2009) Peralkaline nephelinite-natrocarnatite immiscibility and carbonatite assimilation at Oldoinyo Lengai, Tanzania. *Contributions to Mineralogy and Petrology*, **158**, 589–598.
- Mitchell R.H. (2015) Primary and secondary niobium mineral deposits associated with carbonatites. *Ore Geology Reviews*, **64**, 626–641.
- Mitchell R.H. and Gittins J. (2022) Carbonatites and carbothermalites: A revised classification. *Lithos*, **430**, 106861, doi:10.1016/j.lithos.2022.106861.
- Mitchell R.H. and Kjarsgaard B.A. (2004) Solubility of niobium in the system $\text{CaCO}_3\text{--CaF}_2\text{--NaNbO}_3$ at 0.1 GPa pressure: implications for the crystallization of pyrochlore from carbonatite magma. *Contributions to Mineralogy and Petrology*, **148**, 281–287.
- Mitchell R.H. and Smith D.L. (2017) Geology and mineralogy of the Ashram zone carbonatite, Eldor Complex, Quebec. *Ore Geology Reviews*, **86**, 784–806.
- Mitchell R.H., Wahl R. and Cohen A. (2020) Mineralogy and genesis of pyrochlore apatite from The Good Hope Carbonatite, Ontario: A potential niobium deposit. *Mineralogical Magazine*, **84**, 81–91.
- Montero P., Haissen F., Mouttaqi A., Molina J.F., Errami A., Sadki O., Cambeses A. and Bea F. (2016) Contrasting SHRIMP U-Pb zircon ages of two carbonatite complexes from the peri-cratonic terranes of the Reguibat. Implications for the Lateral Extension of the West African Craton. *Gondwana Research*, **38**, 238–250.
- Nasraoui M. and Bilal E. (2000) Pyrochlores from the Lueshe carbonatite complex (Democratic Republic of Congo): a geochemical record of different alteration stages. *Journal of Asian Earth Sciences*, **18**, 237–251.
- Pandit M.K. and Golani P.R. (2001) Reappraisal of the petrologic status of Newania 'carbonatite' of Rajasthan, western India. *Journal of Asian Earth Sciences*, **19**, 305–310.
- Putnis A. (2002) Mineral replacement reactions: from macroscopic observations to microscopic mechanisms. *Mineralogical Magazine*, **66**, 689–708.
- Ramakrishnan M. and Vaidyanandhan R. (2010) *Geology of India, Vol 1 and 2*. Geological Society of India, Bangalore.
- Rampilova M., Doroshkevich A., Viladkar S. and Zubakova E. (2021) Mineralogy of dolomite carbonatites of Sevathur complex, Tamil Nadu, India. *Mineral*, **11**, 355, doi:10.3390/min11040355.
- Ray J.S., Shukla A.D. and Dewangan L.K. (2010) Carbon and oxygen isotopic compositions of Newania Dolomite Carbonatites, Rajasthan, India: implications for source of carbonatites. *Mineralogy and Petrology*, **98**, 269–282.
- Ray J.S., Pande K., Bhutani R., Shukla A.D., Rai V.K., Kumar A., Awasthi A., Smitha R.S. and Panda D.K. (2013) Age and geochemistry of the Newania dolomite carbonatites, India: implications for the source of primary carbonatite magma. *Contributions to Mineralogy and Petrology*, **166**, 1613–1632.
- Reguir E.P., Chakhmouradian A.R., Pisik L., Halden N.M., Yang P., Xu C., Kynický J. and Couëslan C.G. (2012) Trace-element composition and zoning in clinopyroxene-and amphibole-group minerals: implications for element partitioning and evolution of carbonatites. *Lithos*, **128**, 27–45.
- Roy A.B. and Jakhar S.R. (2002) *Geology of Rajasthan (Northwest India): Precambrian to Recent*. Scientific Publishers, 421 pp.
- Sadiq M., Ranjith A. and Umrao R.K. (2014) REE mineralization in the carbonatites of the Sung Valley ultramafic-alkaline-carbonatite complex, Meghalaya, India. *Central European Journal of Geosciences*, **6**, 457–475.
- Samoylov V.S. (1977) *Carbonatites: Facies and Formation Conditions*. Nauka Press, Moscow, Russia [in Russian].
- Schandl E.S. and Gorton M.P. (2004) A textural and geochemical guide to the identification of hydrothermal monazite: criteria for selection of samples for dating epigenetic hydrothermal ore deposits. *Economic Geology*, **99**, 1027–1035.
- Schleicher H., Todt W., Viladkar S.G. and Schmidt F. (1997) Pb/Pb age determinations on the Newania and Sevattur carbonatites of India: evidence for multi-stage histories. *Chemical Geology*, **140**, 261–273.
- Secher K. and Larsen L.M. (1980) Geology and mineralogy of the Sarfartôq carbonatite complex, southern West Greenland. *Lithos*, **13**, 199–212.
- Slezak P. and Spandler C. (2019) Carbonatites as recorders of mantle-derived magmatism and subsequent tectonic events: An example of the Gifford Creek Carbonatite Complex, Western Australia. *Lithos*, **328**, 212–227.
- Sorokhtina N.V., Belyatsky B.V., Zaitsev V.A., Viladkar S.G., Kononkova N.N. and Ghatak A. (2022) New Data on the Age and Genesis of the Newania Carbonatite Complex, Rajasthan, India. *Geochemistry International*, **60**, 1237–1261.
- Tantkar P. (2019) *Geological Investigations of Newania Carbonatite Deposits Udaipur District Rajasthan with Special Reference to Petrogenesis*. PhD Thesis, Mohanlal Sukhadia University, Udaipur, India.
- Trofanenko J., Williams-Jones A.E., Simandl G.J. and Migdisov A.A. (2016) The nature and origin of the REE mineralization in the Wicheeda Carbonatite, British Columbia, Canada. *Economic Geology*, **111**, 199–223.
- Viladkar S.G. (1980) The fenitized aureole of the Newania carbonatite, Rajasthan. *Geological Magazine*, **117**, 285–292.
- Viladkar S.G. and Bismayer U. (2014) U-rich pyrochlore from Sevathur carbonatites, Tamil Nadu. *Journal of the Geological Society of India*, **83**, 175–182.
- Viladkar S.G. and Ghose I. (2002) U-rich pyrochlore in carbonatite of Newania, Rajasthan. *Neues Jahrbuch für Mineralogie-Monatshefte*, **2002**, 97–106.
- Viladkar S.G. and Pawaskar P.B. (1989) Rare earth element abundances in carbonatites and fenites of the Newania complex, Rajasthan, India. *Bulletin of the Geological Survey of Finland*, **61**, 113–122.
- Viladkar S.G. and Subramanian V. (1995) Mineralogy and geochemistry of the carbonatites of the Sevathur and Samalpatti complexes, Tamil Nadu. *Journal of the Geological Society of India*, **45**, 505–505.

- Viladkar S.G. and Wimmenauer W. (1986) Mineralogy and geochemistry of the Newania carbonatite-fenite complex, Rajasthan, India. *Neues Jahrbuch für Mineralogie-Abhandlungen*, **156**, 1–21.
- Viladkar S.G. and Wimmenauer W. (1992) Geochemical and petrological studies on the Amba Dongar carbonatites (Gujarat, India). *Chemie der Erde*, **52**, 277–291.
- Viladkar S.G., Bismayer U. and Zietlow P. (2017) Metamict U-rich pyrochlore of Newania carbonatite, Udaipur, Rajasthan. *Journal of the Geological Society of India*, **89**, 133–138.
- Wallace M.E. and Green D.H. (1988) An experimental determination of primary carbonatite magma composition. *Nature*, **335**, 343–346.
- Watkinson D.H. and Wyllie P.J. (1971) Experimental study of the composition join $\text{NaAlSiO}_4\text{--CaCO}_3\text{--H}_2\text{O}$ and the genesis of Alkalic Rock—Carbonatite Complexes. *Journal of Petrology*, **12**, 357–378.
- Weidendorfer D., Schmidt M.W. and Mattsson H.B. (2017) A common origin of carbonatite magmas. *Geology*, **45**, 507–510.
- Woolley A.R. and Buckley H.A. (1993) Magnesite-siderite series carbonates in the Nkombwa and Newania carbonatite complexes. *South African Journal of Geology*, **96**, 126–130.
- Woolley A.R. and Kjarsgaard B.A. (2008) *Carbonatite Occurrences of the World: Map and Database*. Geological Survey of Canada Open File # 5796, 28 pp.
- Wyllie P.J. and Biggar G.M. (1966) Fractional crystallization in the "Carbonatite Systems" $\text{CaO}\text{--MgO}\text{--CO}_2\text{--H}_2\text{O}$ and $\text{CaO}\text{--CaF}_2\text{--P}_2\text{O}_5\text{--CO}_2\text{--H}_2\text{O}$. Pp 92–105 in: *Papers and Proceedings of the 4th General Meeting - International Mineralogical Association*. Mineralogical Survey of India, New Delhi.
- Wyllie P.J. and Huang W.L. (1975) Influence of mantle CO_2 in the generation of carbonatites and kimberlites. *Nature*, **257**, 297–299.
- Xu C., Kynicky J., Chakhmouradian A.R., Campbell I.H. and Allen C.M. (2010) Trace-element modeling of the magmatic evolution of rare-earth-rich carbonatite from the Miaoya deposit, Central China. *Lithos*, **118**, 145–155.
- Ying J., Zhou X. and Zhang H. (2004) Geochemical and isotopic investigation of the Laiwu-Zibo carbonatites from western Shandong Province, China, and implications for their petrogenesis and enriched mantle source. *Lithos*, **75**, 413–426.
- Zurevinski S.E. and Mitchell R.H. (2004) Extreme compositional variation of pyrochlore-group minerals at the Oka carbonatite complex, Quebec: evidence of magma mixing? *The Canadian Mineralogist*, **42**, 1159–1168.